

## PROBING THE BALANCE OF AGN AND STAR-FORMING ACTIVITY IN THE LOCAL UNIVERSE WITH CHAMP

ANCA CONSTANTIN<sup>1</sup>, PAUL GREEN<sup>1</sup>, TOM ALDCROFT<sup>1</sup>, DONG-WOO KIM<sup>1</sup>, DARYL HAGGARD<sup>2</sup>, WAYNE BARKHOUSE<sup>3</sup>, SCOTT F. ANDERSON<sup>2</sup>

*Draft version June 4, 2018*

### ABSTRACT

The combination of the SDSS and the Chandra Multiwavelength Project (ChaMP) currently offers the largest and most homogeneously selected sample of nearby galaxies for investigating the relation between X-ray nuclear emission, nebular line-emission, black hole masses, and properties of the associated stellar populations. We provide X-ray spectral fits and valid uncertainties for all the galaxies with counts ranging from 2 to 1325 (mean 76, median 19). We present here novel constraints that both X-ray luminosity  $L_X$  and X-ray spectral energy distribution bring to the galaxy evolutionary sequence  $H\ II \rightarrow Seyfert/Transition\ Object \rightarrow LINER \rightarrow Passive$  suggested by optical data. In particular, we show that both  $L_X$  and  $\Gamma$ , the slope of the power-law that best fits the 0.5 - 8 keV spectra, are consistent with a clear decline in the accretion power along the sequence, corresponding to a softening of their spectra. This implies that, at  $z \approx 0$ , or at low luminosity AGN levels, there is an anti-correlation between  $\Gamma$  and  $L/L_{\text{edd}}$ , opposite to the trend exhibited by high  $z$  AGN (quasars). The turning point in the  $\Gamma - L/L_{\text{edd}}$  LLAGN + quasars relation occurs near  $\Gamma \approx 1.5$  and  $L/L_{\text{edd}} \approx 0.01$ . Interestingly, this is identical to what stellar mass X-ray binaries exhibit, indicating that we have probably found the first empirical evidence for an intrinsic switch in the accretion mode, from advection-dominated flows to standard (disk/corona) accretion modes in supermassive black hole accretors, similar to what has been seen and proposed to happen in stellar mass black hole systems. The anti-correlation we find between  $\Gamma$  and  $L/L_{\text{edd}}$  may instead indicate that stronger accretion correlates with greater absorption. Therefore the trend for softer spectra toward more luminous, high redshift, and strongly accreting ( $L/L_{\text{edd}} \gtrsim 0.01$ ) AGN/quasars could simply be the result of strong selection biases reflected in the dearth of type 2 quasar detections.

*Subject headings:* galaxies: active – galaxies: nuclei – galaxies: emission lines – X-rays: galaxies – surveys

### 1. INTRODUCTION: BH ACCRETION, THE LOW LUMINOSITY AGN, AND X-RAY EMISSION

Understanding the nuclear activity in nearby galaxies is essential for constraining the galaxy formation and evolution process. While energetically unimpressive, the nearby galactic nuclei offer the best case scenario for (1) the most common state of accretion in the current universe, (2) the end-point of quasar evolution, or simply (3) their scaled-down version. Observationally, the low redshift  $z \approx 0$  accretion systems are the best testbeds for identifying the processes involved in triggering and further fuelling accretion onto the central black hole (BH) because they offer unique joint investigations of both the nuclear accretion and the properties of the host, i.e., the star-formation (SF).

Unlike the optically luminous quasars, which are radiating close to their Eddington limit (Kollmeier et al. 2006), and only for short ( $\sim 10^7$  yr) times (Yu & Tremaine 2002), accretion activity in nearby galaxy centers appears extremely diverse, spanning  $> 6$  orders of magnitude in the Eddington ratio, and (maybe consequently) a wide range in their duty-

cycles (Heckman et al. 2004; Ho 2008). This variety provides empirical constraints to model predictions linking the BH growth rate and the host bulge formation. The two are indeed connected: it is the younger galaxies that host the more rapidly growing BHs (Heckman et al. 2004; Cid Fernandes et al. 2005; Constantin, Hoyle, & Vogeley 2008). The exact physical mechanism responsible for this link, and in general for the close interplay between SF and BH accretion remains however elusive. Simulations place important constraints on different models for the way black holes are fueled, and provide a quantitative and physical distinction between local, low luminosity, weak (or quiescent) AGN activity, and violent, merger-driven bright quasars (e.g., Hopkins & Hernquist 2006, 2009). Environmental studies of the nearby active galactic nuclei are consistent with these ideas of non-merger-driven fueling for the weak BH growth observed in the nearby universe (Constantin & Vogeley 2006; Constantin, Hoyle, & Vogeley 2008). More recent analysis of the observed distribution of Eddington ratios as a function of the BH masses provide additional constraints, suggesting that even at  $z \approx 0$  there might be two distinct regimes of BH growth, which are determined by the supply of cold gas in the host bulge. The BH regulates its own growth at a rate that is independent of the interstellar medium's characteristics as long as the gas is plentiful, but when the gas runs out the BH's growth will be reg-

<sup>1</sup> Harvard-Smithsonian Center for Astrophysics, Cambridge, MA 02138

<sup>2</sup> Department of Astronomy, University of Washington, Seattle, WA, USA

<sup>3</sup> Department of Physics and Astrophysics, University of North Dakota, Grand Forks, ND 58202, USA

ulated by the rate at which evolved stars lose their mass (Kauffmann & Heckman 2009). These different fueling modes at low luminosities must manifest differently at wavelengths outside the optical regime, allowing further means to constrain and discriminate among them.

The most ubiquitous type of activity at  $z \approx 0$  that resembles that of quasars is identified at optical wavelengths as either a narrow-lined Low Ionization Nuclear Emission Regions (LINER, L) or a “transition” (T) object, whose properties border on the definition of a starburst galaxy and an AGN. Emission-line ratio diagnostics (e.g., Baldwin, Phillips, & Terlevich 1981; Veilleux & Osterbrock 1987; Kewley et al. 2006) that have been quite successful in identifying cases where the dominant ionization mechanism is either accretion onto a black hole (i.e., Seyferts, Ss) or radiation from hot, young stars (i.e., H II nuclei), remain inconclusive for the majority of Ls and Ts. The Ls that exhibit quasar-like broad lines (L1s, by analogy with Seyfert 1s) are unambiguously accretion-powered sources, however those lacking these features (the L2s) could have lines generated by shocks, post-starbursts, or other processes unrelated with accretion. Deciphering the underlying emission source(s) of these ambiguous nuclei is an ongoing struggle.

Recent analyses of the emission properties of the low luminosity AGN (LLAGN) in relation to a wide variety of characteristics of their hosts, together with considerations of their small and large scale environments, reveal a sequence  $H\ II \rightarrow \textit{Seyfert/Transition Object} \rightarrow \textit{LINER} \rightarrow \textit{Passive} (H\ II \rightarrow S/T \rightarrow L \rightarrow P)$  that these objects obey, at least in a statistical sense (Constantin & Vogeley 2006; Schawinski et al. 2007; Constantin et al. 2008). This sequence traces trends in (1) increasing host halo mass, (2) increasing environmental density, (3) increasing central BH mass and host stellar mass, (4) decreasing BH accretion rate, (5) aging of the stellar population associated with their nuclei, and (6) decreasing in the amount of dust obscuration, which might translate into a decrease in the amount of material available for star-forming or accretion. This sequence therefore suggests a process of transformation of galaxies from SF via AGN to quiescence, which may be the first empirical evidence for an analogous duty cycle to that of the high  $z$  bright systems (i.e., quasars). State of the art hydrodynamical models provide clear support for such a scenario, by showing that during mergers, the BH accretion peaks considerably *after* the merger started, and *after* the star-formation rate has peaked (e.g., Di Matteo et al. 2005; Hopkins et al. 2006). Constraining the nature of this  $H\ II \rightarrow S/T \rightarrow L$  sequence at  $z \approx 0$  will improve our understanding of the degree to which the LLAGN phenomenon fits into the galactic BH accretion paradigm.

The X-ray emission is, arguably, the most sensitive test for accretion and its intensity and efficiency, and thus, it is of great interest to test and validate this sequence against large homogeneous X-ray selected samples. The Chandra Multiwavelength Project (ChaMP; Green et al. 2004) provides a unique opportunity for this, by providing the largest-area Chandra survey to date, which, when cross-matched with the SDSS, provides an unprecedented number of galaxies in the local Universe for which we can combine and contrast measurements of the X-ray and optical emission. The sample of  $\sim 110$  Chandra X-ray

detected nearby galaxies (excluding broad line objects) analysed in this study represents a significant improvement in both sample size and homogeneity both for X-ray selection and optical spectral type coverage.

Previous studies of the relation between the X-ray nuclear emission, optical emission line activity and black hole masses provide important physical constraints to the LLAGN phenomenon. Almost invariably, the conclusions are that LLAGN are probably scaled down versions of more luminous AGN (e.g., Ho et al. 2001; Panessa et al. 2006), and that  $M_{\text{BH}}$  is not the main driver of the (soft) X-ray properties (Greene & Ho 2007). The LLAGN are claimed to be X-ray detected at relatively high rates, and are found to be relatively unabsorbed, obscuration appearing to play only a minor role in their detection rates and/or in classifying them as types 1 and 2 in X-rays (Roberts & Warwick 2000; Halderson et al. 2001; Miniutti et al. 2008; Ho 2008), with the exception of those known to be Compton thick. Nonetheless, the X-ray investigations of AGN activity at its lowest levels remain largely restricted to Ls and Ss.

Deciphering the ambiguous nature of Ls in particular, has been the target of many X-ray studies of LLAGN focused on these sources (Yaqoob et al. 1995; Ishisaki et al. 1996; Iyomoto et al. 1998, 2001; Terashima et al. 1998, 2000a,b, 2002; Pellegrini et al. 2000a,b, 2002; Georgantopoulos et al. 2002; Ptak et al. 1996, 1999, 2004; Roberts, Schurch & Warwick 2000). A hard, power-law AGN signal is generally *spectrally* resolved for the majority of them, however, the corresponding energy (photon) index is marginally steeper (softer) than in (broad line) Ss; many of them require a soft thermal component, that somehow differs from the blackbody soft excess commonly seen in Ss and quasars. The Fe  $K\alpha$  emission or the Compton reflection component are usually weak in these sources, indicating that X-ray reprocessing is not by material in an optically thick accretion disk (Lightman & White 1988; George & Fabian 1991). Because most of these studies are based on large-beam observations, mostly *ASCA* or *BeppoSAX*, Ls’ emission has also quite often been attributed to stellar processes. Higher spatial resolution *Chandra* and *XMM-Newton* observations (Bohringer et al. 2001; Kim & Fabbiano 2003; Pellegrini et al. 2003; Terashima & Wilson 2003; Filho et al. 2004; Page et al. 2004; Starling et al. 2005; Flohic et al. 2006; Gonzalez-Martin et al. 2006; Soria et al. 2006) remain torn between these findings, as the stellar interpretation persists for quite a number of these sources.

In this work we approach the LLAGN phenomenon via the  $H\ II \rightarrow S/T \rightarrow L \rightarrow \textit{Passive}$  galaxy evolutionary sequence described above. In particular, we test the validity of the sequence within X-ray selected LLAGN via a large variety of optical emission properties, which first provided evidence for the sequence, and also in their X-ray properties. We combine the ChaMP X-ray detections with a sample of SDSS DR4 nearby galaxies that excludes broad line objects, creating a large sample of galaxy nuclei that spans a range of spectral types, from passive to actively line emitting systems, including the star-forming and accreting types, along with those of mixed or ambiguous ionization. Through measurements

of their X-ray spectra<sup>4</sup>, fluxes and luminosities, we characterize the sequence in terms of strength and mode of accretion. We provide here the first investigation of the relation between  $\Gamma$  and the Eddington ratio  $L/L_{\text{edd}}$  at the lowest levels of accretion. We reveal a rather surprising anti-correlation between these two measures, opposite to what luminous AGN and quasars exhibit. This finding reveals a turning point in the general  $\Gamma - L/L_{\text{edd}}$  relation followed by AGN, which is identical (within the errors) to that shown by the  $\Gamma - L/L_{\text{edd}}$  trends in black hole X-ray Binaries (XRBs).

Throughout this work we assume  $\Omega_m = 0.3$ ,  $\Omega_\Lambda = 0.7$ , and  $H_0 = 70 h \text{ km s}^{-1} \text{ Mpc}^{-1}$ .

## 2. THE CHAMP-BASED LLAGN SAMPLE

The sample of LLAGN employed in this study is obtained by cross-matching the SDSS DR4 spectroscopic sample of galaxies with the X-ray detected sources identified as part of the *Chandra* Multiwavelength Project (ChaMP). ChaMP is a wide-area serendipitous X-ray survey based on archival X-ray images of the  $|b| > 20$  deg sky, obtained with *Chandra*'s AXAF CCD Imaging spectrometer (ACIS). A summary of the survey is presented in Green et al. (2004) and Green et al. (2009), while ChaMP results and data can be found at <http://hea-www.harvard.edu/CHAMP>. The X-ray analysis extends to a total of 392 fields through *Chandra* Cycle 6, that cover a total of  $\sim 30 \text{ deg}^2$  of sky area.

We limit the investigation to the DR4 dataset in order to employ the measurements of absorption and emission line fluxes and equivalent widths (EW) drawn from the catalog built by the MPA/JHU collaboration<sup>5</sup>. Here the line emission component is separated and subtracted from the total galaxy spectrum based on fits of stellar population synthesis templates (Tremonti et al. 2004). The catalog does not include broad-line objects. To relate the central BH accretion activity to the host properties, we employ stellar masses of galaxies and the  $H\delta_A$  Balmer absorption-line index as a proxy for the age of the associated stellar population, as calculated and presented by Kauffmann et al. (2003b). A detailed analysis of these properties, and their relation to the AGN phenomenon revealed through optical signatures, are presented in Kauffmann et al. (2004).

The cross-match of all ChaMP sky regions imaged by ACIS with the SDSS DR4 spectroscopic footprint results in a parent sample of 15955 galaxies on or near a chip, and a subset of 199 sources that are X-ray detected. Among those, only 107 sources have an off-axis angle (OAA)  $\theta < 0.2 \text{ deg.}$  and avoid  $ccd = 8$  due to high serial readout noise; these objects comprise the main sample we employ for this study. Subsequent subsections present details of the X-ray spectral analysis, together with a presentation of their general optical and X-ray properties, the definition of the subsamples based on their optical spectral properties, and a discussion of the selection effects associated with these samples.

### 2.1. X-ray spectral analysis

<sup>4</sup> i.e., the shape of the spectral energy distribution quantified by the photon index  $\Gamma$  that best fits a power-law  $N(E) \propto E^{-\Gamma}$

<sup>5</sup> publicly available at <http://www.mpa-garching.mpg.de/SDSS/> (Brinchmann et al. 2004)

*Chandra* imaging with ACIS provides energy resolution sufficient to constrain the X-ray spectral properties as well. To characterize the X-ray activity of the ChaMP-SDSS galaxies included in our sample, we perform direct spectral fits to the counts distribution using the full instrument calibration, known redshift and Galactic 21cm column<sup>6</sup>  $N_H^{\text{Gal}}$ . Source spectra are extracted from circular regions with radii corresponding to energy encircled fractions of  $\sim 90\%$ , while the background region encompasses a  $20''$  annulus, centered on the source, with separation  $4''$ , from the source region. Any nearby sources are excised, both from the source and the background regions.

The spectral fitting is done via `yaxx`<sup>7</sup> (Aldcroft 2006), an automated script that employs the CIAO *Sherpa*<sup>8</sup> tool. Each spectrum is fitted in the range  $0.5 - 8 \text{ keV}$  by two different models: (1) a single power-law plus absorption fixed at the Galactic 21cm value: (model "PL"), and (2) a fixed power-law of photon index  $\Gamma = 1.9$  plus intrinsic absorption of column  $N_H$  (model "PLfix"). These fits use the Powell optimization method, and provide a robust and reliable one-parameter characterization of the spectral shape for any number of counts. Spectra with less than 100 net counts were fit using the ungrouped data with Cash statistics (Cash 1979), while those with more than 100 counts were grouped to a minimum of 16 counts per bin and fit using the  $\chi^2$  statistic with variance computed from the data. For the (9) objects with more than 200 counts we employ a third model where both the slope of the power-law and the intrinsic absorption are free to vary (model "PLabs").

Many of the X-ray detected galaxies in our sample have relatively few net counts (mean 76, median 19). In such cases, instrumental hardness ratios is often used, in the belief that genuine spectra fitting is not warranted by the data quality. We stress however that spectral fitting provides the most consistent and robust estimates of the physical parameters of interest, the power law slope and intrinsic absorption. Because the ChaMP X-ray exposures span a variety of intervening Galactic columns, include data from both back- and front-side ACIS CCDs, and span 6 years of observations, the spectral response between sources varies significantly. While constraints from spectral fitting may not be tight for low count sources, use of unbinned event data and the appropriate response gives an optimal and unbiased estimate of the fit parameters and their uncertainties, especially important when absorption may be present at different redshifts. Classical hardness ratio analysis on the other hand amounts to grouping the data into two rather arbitrary bins, introducing potential biases and statistical complexity. Interpreting the hardness ratio value for ChaMP sources in disparate fields requires incorporating the instrument response in any case, so we strongly prefer spectral fitting. Nevertheless, when there is only one free parameter, only the overall spectral shape is constrained.

This simple parametrization proves generally sufficient to model the  $0.5 - 8 \text{ keV}$  spectra of these objects. Com-

<sup>6</sup> Neutral Galactic column density  $N_H^{\text{Gal}}$  taken from Dickey & Lockman (1990) for the *Chandra* aimpoint position on the sky.

<sup>7</sup> <http://cxc.harvard.edu/contrib/yaxx>

<sup>8</sup> <http://cxc.harvard.edu/sherpa>

parisons of 0.5 – 8 keV fluxes  $f_x$  (and luminosities  $L_X$ ) obtained from the PL and PLfix models show good agreement, for the whole sample of galaxies, the average (median) of the difference in these values being 0.07 (0.01) dex. We caution that the simple power-law fits we use here could be misleading for objects where the absorption is complex (i.e., a partial covering, with one or more absorber potentially being ionized). However, the data quality is insufficient to show that the situation is more complex than a simple power-law.

We compile a set of "best" measurements for  $\Gamma$  or  $N_H$ , by using the values obtained from the PL (intrinsic  $N_H$  fixed at zero) and PLfix ( $\Gamma$  fixed at 1.9) models, respectively. For objects with more than 200 counts we use the  $\Gamma$  and  $N_H$  values obtained from the PLabs. The mean  $\Gamma$  for the whole sample of 107 galaxies is  $2.03 \pm 1.38$ , with a median of 2.04. The level of intrinsic absorption is generally low. More than 85% of the sample exhibits  $N_H < 1 \times 10^{22} \text{ cm}^{-2}$ , while for 60% of the objects the spectral fits are consistent with zero intrinsic absorption. Note that, given the simplified model used in fitting the X-ray spectra, these values might not necessarily represent the true distribution of absorption in these objects. Individual measurements of all of these X-ray properties, together with their observational parameters, like the total number of X-ray counts, the exposure time, the off-axis angle, together with their corresponding X-ray source ID, are listed in Table 1 for all 107 objects.

Contribution from thermal emission is expected for some of the objects included in this sample of nearby galaxies, whether or not they show line emission activity. Such a component may provide a reasonable contribution to the total (X-ray) emission even in objects where the dominant ionization mechanism, as identified optically, is a compact nuclear source, i.e., an AGN. LINERs, for instance, have frequently been associated with photoionization by hot, young stars (Filippenko & Terlevich 1992; Shields 1992; Barth & Shields 2000), clusters of planetary nebula nuclei (Taniguchi, Shioya, & Murayama 2000), or more recently (and perhaps more consistent with their older stellar populations), by hot post-AGB stars and white dwarfs (Stasinka et al. 2008).

We attempted fitting the 0.5 – 8 keV spectra with a Raymond-Smith (R-S) thermal plasma model, with the abundance fixed at 0.5 solar. The choice of abundance level is inspired by previous investigations of LLAGN, e.g., Ptak et al. (1999) and Terashima et al. (2002), even though in many cases the abundance remains poorly constrained. This R-S model fit results seem physically feasible for only about the third of the sample. Reasonable values, in agreement with previous findings, i.e.,  $kT \lesssim 2 \text{ keV}$  are only found for 35 sources. For another third the best fit  $kT > 10 \text{ keV}$ . We discuss in more detail the results of fitting this model as a function of the optical spectroscopic properties of these sources in Section 2.5.

As probably expected, it is the passive galaxies that show the softest power-law slopes we measure ( $\Gamma > 3.5$ ), suggesting that, for these cases in particular, a power-law representation may be incorrect. If we instead fit a Raymond-Smith model, we derive reasonable typical temperatures near  $\sim 0.7 \text{ keV}$ . Nonetheless, since even these objects are likely to have some power-law contribution from X-ray binaries, the R-S model is perhaps

no better a characterization of the true spectrum than a power-law. The X-ray flux distribution we derive from the R-S model fits to passive galaxies is not significantly different ( $\pm 25\%$ ), so we prefer to retain the power-law fits everywhere to facilitate more direct comparison of the different spectral classes.

## 2.2. The Optical Spectral Classification

We identify and classify accretion sources and other types of active systems in both the parent galaxy sample and the X-ray detected subsample, based on their optical emission line properties. It has been argued (Ho, Filippenko, & Sargent 1997a; Constantin & Vogeley 2006; Kewley et al. 2006) that the best way to separate accretion sources from starbursts or other types of active systems is via a set of three diagnostic diagrams, which employ four line flux ratios:  $[\text{O III}]\lambda 5007/\text{H}\beta$ ,  $[\text{N II}]\lambda 6583/\text{H}\alpha$ ,  $[\text{S II}]\lambda\lambda 6716, 6731/\text{H}\alpha$ , and  $[\text{O I}]\lambda 6300/\text{H}\alpha$ . Thus, for both samples, we first select a subset of strong emission-line sources that show significant emission in all six lines used in the type classification ( $\text{H}\alpha$ ,  $\text{H}\beta$ ,  $[\text{O III}]$ ,  $[\text{N II}]$ ,  $[\text{S II}]$ , and  $[\text{O I}]$ ), and a set of passive objects that show insignificant line emission activity. An emission feature is considered to be significant if its line flux is positive and is measured with at least  $2\sigma$  confidence. Following Kewley et al. (2006) classification criteria, the emission-line objects are separated into Seyferts (Ss), LINERs (Ls), Transition objects (Ts), and star-forming, or H II galaxy nuclei.

This method of classifying low luminosity actively line-emitting galaxy nuclei has the disadvantage that it leaves unclassified a high fraction ( $\sim 40\%$ ) of galaxies, which show strong emission features, but not in all six lines considered here. The condition for strong emission in  $[\text{O I}]$  in particular is significantly restrictive. Moreover, another quite large ( $\sim 25\%$ ) fraction of the emission-line objects remains unclassified, as their line ratios, although accurately measured, do not correspond to a clear spectral type in all three diagrams. In the majority of such cases, while the  $[\text{N II}]/\text{H}\alpha$  ratio shows relatively high, S-like values, the corresponding  $[\text{S II}]/\text{H}\alpha$  and/or  $[\text{O I}]/\text{H}\alpha$  place them in the T or H II-like object regime; thus, because the  $[\text{S II}]$  and  $[\text{O I}]$  emission lines are better AGN-diagnostics than  $[\text{N II}]$ , these systems are likely to be excluded from the AGN samples selected via these classifications. As a consequence, our samples based on the 6-line classification are small.

To enlarge our samples of galaxy nuclei of all spectral types, we also explored an emission-line classification based on only the  $[\text{O III}]/\text{H}\beta$  vs.  $[\text{N II}]/\text{H}\alpha$  diagram, i.e., a 4-line classification method, for the X-ray detected sources. The emission line galaxy samples comprise thus all objects showing at least  $2\sigma$  confidence in the line flux measurements of these four lines only. The delimitation criteria of H II's and T's remain unchanged, while Ss and Ls are defined to be all objects situated above the Kewley et al. (2006) separation line, and with  $[\text{O III}]/\text{H}\beta > 3$  and  $< 3$  respectively. The 4-line and 6-line classifications result in significantly different classes when applied to optically selected galaxies in general (Constantin & Vogeley 2006). In particular, true properties become heavily blended into the dominant population of LINERs (or Ts, depending on the sepa-

ration lines used in the diagnostic diagrams). Interestingly, however, when applied to the X-ray sample, the 4-line classes fall well within the 6-line loci; although Ss and Ls are separated only by their  $[\text{O III}]/\text{H}\beta$  line flux ratio, they remain clearly separated into the  $[\text{S II}]/\text{H}\alpha$  and  $[\text{O I}]/\text{H}\alpha$  diagrams as well. Figure 1 shows how the 6-line (top) and the 4-line (bottom) classifications compare for the ChaMP X-ray detected galaxies.

Although the sample of X-ray detected galaxies is small, this comparison indicates that adding X-ray detection makes the 4-line classification more secure, and that the need for the (usually unavailable)  $[\text{O III}]/\text{H}\beta$  vs.  $[\text{S II}]/\text{H}\alpha$ , and  $[\text{O III}]/\text{H}\beta$  vs.  $[\text{O I}]/\text{H}\alpha$  diagrams is not as stringent as in the cases where only optical information is available. We will thus consider for the analysis presented in this paper only the 4-line classification.

### 2.3. The X-ray detection fraction of the LLAGN

The "cleaning" role of the X-ray detection in finding and defining LLAGN is even more obvious when we compare the fractions of X-ray detected objects by spectral type, both relative to the parent sample of nearby optically selected objects and the subsample of X-ray detected galaxies. Table 2 lists these percentages, where for the parent optically selected sample we consider only the SDSS galaxies on ACIS chips (excluding chip S4, *ccd#8*), and with off-axis angle  $\theta < 0.2$  deg, consistent with the conditions used in compiling the X-ray samples. The first two columns show the number (and fraction) that each spectral type represents, among (1) the optical parent sample and (2) the X-ray-detected subsample. The third column lists the raw fraction of X-ray detections per spectral type.

That the X-ray detection is very efficient in finding LLAGN, particularly Seyferts, is quite apparent. While narrow-line Ss usually make up only  $< 2 - 4\%$  (Ho, Filippenko, & Sargent 1997b; Constantin & Vogeley 2006) of the optically selected nearby galaxies, the X-ray detection increases the chances of finding them tenfold. Ts and Ls, where an AGN contribution to the total ionization power is expected, are also much better represented in the X-ray detected sample of galaxies, their fractions being  $\sim 3\times$  larger than when only optical selection is employed. Some 65% of the optically defined Ss are detected in X-rays, while the other spectral types hardly reach an X-ray detection fraction of 20%. Ls are the second most X-ray active sources within nearby galaxies, while Ts and the galaxies that show some/weak emission line activity account for less than 1/5th of the sample. As we discuss further in Section 2.5, only the luminous H IIs are detected in X-rays. While the X-ray detection rate of the H IIs is basically consistent with zero, when detected, their X-ray emission is moderately strong,  $L_X = 10^{39} - 2.5 \times 10^{41}$  erg  $\text{s}^{-1}$ ; half of the H II detections show X-ray luminosities higher than the level that can be reached without contribution from AGN ( $10^{40}$  erg  $\text{s}^{-1}$ ), suggesting once more that the nuclear emission in these sources might not be completely driven by stellar processes.

The only previous studies that encompass the whole spectral variety of LLAGN are Roberts & Warwick (2000) and Parejko et al. (2008), which employ ROSAT (HRI and RASS respectively). Their search for X-ray

emitting nearby galaxy nuclei, optically characterized via the Palomar and SDSS surveys respectively, concluded in soft X-ray detection rates of  $\sim 70\%$  of both Ss and Ls (HRI),  $\sim 70\%$  of Ss and  $\sim 60\%$  Ls (RASS),  $\sim 40\%$  (HRI) and  $< 10\%$  (RASS) of H II's, and  $\sim 30\%$  of passive galaxies (both cases). Comparison of these detection rates to ours is problematic, because of their softer instrument bandpass, lower sensitivity, but wider sky coverage.

Hard X-ray studies of homogeneously selected samples including all spectral types of nearby active galaxies are practically non-existent. Ls, and particularly those found in the Palomar survey, have been clearly privileged in terms of X-ray targeting (e.g., Ho et al. 2001). Their detection rates are found to be significantly higher than what we report here based on the serendipitous ChaMP survey. Ho et al. (2001) reports a  $\sim 70\%$  detection rate, while, when chosen for having a flat-spectrum radio core, Ls are found to be 100% X-ray active (Terashima & Wilson 2003). Later studies claiming better accounting for selection and classification as LINER (Satyapal et al. 2004; Dudik et al. 2005; Pellegrini 2005; Satyapal et al. 2005; Flohic et al. 2006; Gonzalez-Martin et al. 2006) conclude with lower fractions,  $\sim 50\%$ .

ChaMP has the distinct advantage of presenting a large, homogeneous serendipitous sample of LLAGN. The detection fraction is not an intrinsic property of galaxies, but rather a convolution of galaxy properties with optical survey depth, and the X-ray sensitivity vs. sky area curve. As described in (Green et al. 2009), the ChaMP is characterising the X-ray sensitivity at the position of every SDSS galaxy, which will enable us to compile the unbiased fraction of galaxies by optical spectral type (e.g., Ls) that fall in X-ray luminosity bins, from sky volumes complete to those limits. We will present the results of such an investigation in a subsequent paper.

### 2.4. Selection Effects: the ChaMP X-ray Galaxy Sample is Minimally Biased

X-ray and optical emission are correlated. Thus, while the X-ray selection is one of the most powerful tools to exploit in detecting accretion sources, it is also expected that this selection picks up, selectively, the brightest (optical) sources. Due to its serendipitous character, ChaMP should however reduce such effects. Note that, out of 107 X-ray detections that this ChaMP sample of galaxies provides, only 13 are targets.

We explore in Figure 2 the biases that X-ray detection potentially adds to our sample. Comparisons of the distributions of redshift  $z$ , apparent and absolute  $r$ -band (SDSS) magnitudes,  $r$  and  $M_r$ , respectively, and of the concentration index  $C^9$  as a proxy for the morphological type of these galaxies. Both for the whole optically and X-ray selected samples (histograms on the left panel) and separately per spectral type (the right panel) show, pleasingly, that biases are not strong.

However, H II galaxies are of lower  $z$  and brighter  $M_r$  when detected in X-ray. As shown in the next section, the H IIs are generally weak X-ray sources. The tendency for X-ray detected galaxies to appear brighter in appar-

<sup>9</sup>  $C = R_{50}/R_{90}$ , where  $R_{50}$  and  $R_{90}$  are the radii from the center of a galaxy containing 50% and 90% of the Petrosian flux

ent magnitude ( $r$ , by  $\sim 0.5$  mag) seems to be caused by the large difference in  $r$  between the H II galaxies alone, as all the other types of sources show very similar ranges, averages or medians, when analysed separately.

The concentration index  $C$  appears to be somewhat larger for the X-ray objects. Several factors are likely to account for this. The H IIs are the least concentrated optically, and have the lowest X-ray detection fraction. X-ray detection is sensitive to the AGN activity, which is more prevalent in the early type (massive bulge-dominated) galaxies (e.g., Ho, Filippenko, & Sargent 2003; Kauffmann et al. 2004). Nuclear activity is also expected to increase  $C$  simply by adding light to the core. Note that there is no significant difference in this parameter in regard to Ss’ X-ray selection. However, Ss make up for a tiny fraction of  $z \approx 0$  galaxies, and the morphology of their hosts spans quite a range.

### 2.5. General X-ray Properties in Relation to Optical Spectroscopic Classification

X-ray information about the nearby galaxy centers constrains the contribution of accretion-related processes to their optical spectral characteristics. We present in this section the distributions of a variety of X-ray properties for the whole sample as well as for subsamples by optical spectral class. Figure 3 shows the distributions of the X-ray counts, the  $0.5 - 8$  keV unabsorbed X-ray fluxes, the best-fit X-ray photon indices  $\Gamma$  and the intrinsic neutral hydrogen column densities  $N_H$ . These measurements are shown for the whole sample of X-ray detected nearby galaxy nuclei (left column), and separately per spectral type (right column).

For X-ray fluxes, we show the values derived using the primary power-law fitting models discussed in Section 2.1: (1) a single power-law with no intrinsic absorption and (2) a fixed power-law ( $\Gamma = 1.9$ ) with absorption. The  $f_x$  values are generally consistent with each other for the whole range of brightness and optical spectral type. As expected, the X-ray brightest objects are among Ss, however, even for this spectral type the range of values remains pretty broad, spanning 3 orders of magnitude. Note also that the few H II galaxies that are X-ray detected are in general brighter than the passive systems.

In terms of the X-ray spectral shape, the ChaMP nearby galaxies are quite a diverse population. The mean photon index per optical spectral type shows however a rather clear dependence on the spectral type: Ss show the hardest  $0.5 - 8$  keV spectral shape, becoming softer and softer from Ts to Ls to the Passive galaxies which are clearly the softest. The H II galaxies are unexpectedly hard in average  $\Gamma = 1.46$ , however, two particularly hard detections clearly weight the subsample in this direction. The Ts and Ls average at  $\Gamma \approx 2$ .

The  $N_H$  values are poorly constrained for this sample, and there is no obvious correlation with the optical spectral type. It is however obvious that the Ss are the sources with the highest fraction of non-zero absorption. Since all our Ss are of type 2, i.e., lack broad emission lines in their spectra, the unification paradigm predicts that many will show signature of absorption in X-rays. A typical unabsorbed power-law  $\Gamma = 1.9$  requires a column density of  $N_H = 8 \times 10^{21} \text{ cm}^{-2}$  to yield an apparent  $\Gamma = 1$  similar to the mean value found for our S subsample, which is consistent with the observed mean  $N_H$  for

these particular systems.

## 3. PROBING THE SEQUENCE

The  $H \text{ II} \rightarrow S/T \rightarrow L$  evolutionary sequence proposes a comprehensive picture for the co-evolution of AGN and their host galaxies. This scenario is supported by and strengthens previous studies of AGN, star-formation activity and their co-evolution in nearby galaxies (Kauffmann et al. 2004; Heckman et al. 2004), and may enhance our understanding of how AGN work and evolve in relation to both their hosts and their environments (Constantin, Hoyle, & Vogeley 2008).

X-rays, as primary signatures of supermassive BH accretion, offer a critical verification of the proposed sequence.  $L_X$  and spectral fits characterize the sequence in terms of strength and mode of accretion, especially the order of Ss and Ts within the  $H \text{ II} \rightarrow S/T \rightarrow L$  cycle. Both the bulge nebular properties, and the small and large scale environments of Ss and Ts, are very similar and remain intermediate between those of H IIs and Ls. The only parameters showing a “jump” in the otherwise smooth trends are  $H\alpha/H\beta$  Balmer decrements and the nearest neighbor distance  $d_{1\text{nn}}$  (Constantin, Hoyle, & Vogeley 2008).  $H\alpha/H\beta$  provides a measure of absorption, and perhaps also the amount of fuel available for accretion, which we can now test directly against both  $L_X$  (accretion power) and X-ray spectral constraints.

We present in Figure 4 a comparison of the degree to which optically and X-ray selected galaxies follow the proposed sequence in terms of the black hole mass  $M_{\text{BH}}$ , obtained via  $\sigma_*$  measurements and the  $M_{\text{BH}} - \sigma_*$  relation (Tremaine et al. 2002), the (dust corrected) stellar mass  $M^*$  (Kauffmann et al. 2003a), the Balmer decrement  $H\alpha/H\beta$  as a proxy for dust extinction, the  $H\delta_A$  Balmer absorption index as a measure of the age of the associated stellar population,  $L[\text{OIII}]$ , and the accretion rate expressed as  $L/L_{\text{edd}}$ , where  $L = L_{\text{bol}} = 600 \times L[\text{OIII}]$  for the bolometric correction (Heckman et al. 2004; Kauffmann & Heckman 2009), and the  $L[\text{OIII}]$  is extinction-corrected using the corresponding Balmer decrements and a  $\tau \propto \lambda^{-0.7}$  attenuation law (Charlot & Fall 2000). Given the (spectral) definition of passive galaxies (i.e., lacking optical emission line activity), there are no measurements of the Balmer decrement,  $L[\text{OIII}]$  and  $L/L_{\text{edd}}$  for these sources. It is notable that in all measures, and for all types of sources, the X-ray and optically selected sources are very similar, and appear to obey the  $S \rightarrow T \rightarrow L \rightarrow P$  sequence.

If anything, the sequence appears stronger among the X-ray selected galaxies, both in median/average values and in their distributions of individual measurements, which span smaller ranges of values than for the optically selected objects. Among the weakest accreting objects, Ls and Passive galaxies, the X-ray selection tends to pick up more massive objects, with heavier BHs, and older stellar populations; there is however no obvious difference in these parameters for the other types of sources. As expected, these massive systems also appear to have smaller [O III] luminosities and accretion rates, accentuating the sequential  $S$  to  $T$  to  $L$  drop in these parameters suggested by optically selected/defined objects. Also, while the Balmer decrement distributions suggest that,

in general, the X-ray selection is not strongly affected by dust, the slightly more obscured X-ray detected H IIs and less obscured X-ray detected Ls make the sequence more apparent.

Figure 5 illustrates how the 0.5 - 8 keV X-ray luminosity  $L_X$  and the corresponding  $L/L_{\text{edd}}$  behavior along the  $S \rightarrow T \rightarrow L \rightarrow P$  sequence. For the sake of comparison, we show  $L_X$  values obtained via two spectral fitting models, 1. a power-law with no intrinsic absorption (only the Galactic one) and 2. a fixed power-law with  $\Gamma = 1.9$  and with variable intrinsic absorption added to the Galactic level. The sequence is supported by both types of measurements, albeit stronger when the simple power-law model is used. As discussed in Sections 2.1 and 2.5, the free power-law with no intrinsic absorption spectral model, that seems to best characterize this sample of objects, makes the statistical sequence even more probable. For the sequence in the accretion rate, we calculate  $L/L_{\text{edd}}$  using  $L/L_X = 16$  for the bolometric luminosity, as suggested by Ho (2008), and the BH masses estimated from their host stellar velocity dispersion  $\sigma_*$  using Tremaine et al. (2002). We also contrast the X-ray measurements with those where  $L_{\text{bol}}$  derived from  $L[\text{OIII}]$ ; note that while  $L_X$  and the derived  $L/L_{\text{edd}}$  are available for the whole sample of 107 objects, only 69 of them exhibit strong 2- $\sigma$  detectable, [O III] line emission. The  $S \rightarrow T \rightarrow L \rightarrow P$  galaxy sequence compares well in both optical and X-ray measurements. The values of all these parameters decrease monotonically in both median and average values, from Ss to Ts, to Ls and Passive galaxies, consistent with what optical properties of these sources put forward.

The H IIs are the only apparent exception here. The small number statistics for these galaxy nuclei preclude any strong conclusions. Given the expected high sensitivity to soft sources that these measurements provide, their spectra tend to be on the hard side. Obscuration is a notorious cause for spectral hardening, and thus, the possibility that these objects hide in their centers obscured BH accretion is still not ruled out.

Note also that the power-law slope  $\Gamma$  that best fits the X-ray spectra increases from Ss to Ts, to Ls, in both median and average values, showing a tendency of softening of the spectra from Ss to passive galaxies along the proposed sequence (Figure 3). This is quite an interesting finding, as in other AGN, mostly the luminous type 1 AGN, observations suggest an opposite trend: the stronger accreting (and more luminous) sources are the softer ones, most recently quantified by Kelly et al. (2008); Shemmer et al. (2008). It is interesting to note that a spectral softening with strengthening of the accretion process/rate is also a generally common feature of the X-ray Binaries (XRBs) with reasonably high  $L/L_{\text{edd}}$  (e.g., Kubota & Makishima 2004). Note however that, when the Eddington ratio is less than a critical value,  $L/L_{\text{edd}} \lesssim 0.01$ , i.e., XRBs are observed in their low/hard state, there is a clear trend for softening with further weakening of the accretion rate (Kalemci et al. 2005; e.g., Yamaoka et al. 2005; Yuan et al. 2007). We investigate this finding in more detail in the following section, and discuss the analogy with the XRB phenomenon.

Investigations of how X-ray parameters depend on the accretion rate relative to the Eddington rate are expected to offer important constraints on physical models of the AGN X-ray emitting plasma, particularly its geometry. A hot, optically thin corona that Compton up-scatters UV photons from the optically thick disk (Shakura & Syunyaev 1973; Haardt & Maraschi 1991) seems to fit reasonably well the X-ray emission of the highly accreting systems, particularly when it is associated with a hot, possibly patchy and "skin"-like structure "sandwich"-ing the cold disk (Nayakshin 2000; Czerny et al. 2003). Other geometries remain however viable, among them an accretion disk evaporating into a hot inner flow (Shapiro et al. 1976; Zdziarski et al. 1999), or combinations of a hot inner flow and the patchy corona (Poutanen et al. 1997; Sobolewska et al. 2004). For LLAGN, with  $L/L_{\text{edd}} < 10^{-9} - 10^{-5}$ , the accretion flow has been hypothesized to originate from a geometrically thick and hot disk-like structure that is inefficient at converting gravitational potential energy into radiation, the radiatively inefficient accretion flow (RIAF) model (e.g., Narayan & Yi 1994; Blandford & Begelman 1999; Narayan et al. 2000). Models suggest that there is a transition/switch from a standard disk to an advection dominated accretion flow (ADAF; or, a radiatively inefficient accretion flow, RIAF) when  $L/L_{\text{edd}}$  declines below a critical value within a certain transition radius (Esin et al. 1997; Yuan & Narayan 2004; Lu et al. 2004). In either case, radiation pressure driven outflows can also alter the physics of the corona (Proga 2005). Because the efficiency in producing an X-ray accretion flow and in driving the outflows depends on the BH mass and its accretion rate, it is important to understand the interdependence of these parameters on the X-ray properties, particularly the shape of the X-ray spectrum, i.e., the X-ray photon index  $\Gamma$ .

The relationship between  $\Gamma$  and the Eddington ratio  $L/L_{\text{edd}}$  is relatively well studied, and yet a controversial issue. These two parameters seem to be positively correlated for objects accreting at relatively high Eddington ratios, i.e., quasars, luminous type 1 Seyferts (Kelly et al. 2008; Shemmer et al. 2008), while for low  $L/L_{\text{edd}}$  values the situation remains uncertain, mainly due to the lack of quality data in that regime. The conclusion so far seems to be that the shape of the hard X-ray power-law is largely controlled by  $L/L_{\text{edd}}$ . For the luminous, strongly/efficiently accreting sources, it is proposed that the corona acts as a "thermostat" by (Compton) cooling more efficiently when the disk emission increases, producing more soft photons, and thus steepening the hard X-ray spectrum. This scenario also accounts nicely for the generally narrow range of  $L/L_{\text{edd}}$  and  $\Gamma$  values measured in (optically selected) quasars or luminous AGN, in general [ $L/L_{\text{edd}} \sim 0.3$  with a typical dispersion of a factor of  $\sim 5$ ; (McLure & Dunlop 2004; Kollmeier et al. 2006; Netzer et al. 2007; Shen et al. 2008).  $\Gamma \sim 1.5 - 2.5$ ; (Vignali et al. 2005; Shemmer et al. 2008)]. For LLAGN, the  $\Gamma - L/L_{\text{edd}}$  relation remains only vaguely constrained.

The relation between the X-ray photon index  $\Gamma$  and the Eddington ratio for the ChaMP X-ray detected galaxies is illustrated in Figure 6. The Eddington luminosity  $L_{\text{edd}}$  is calculated as indicated in Section 3, using  $M_{\text{BH}}$  values estimated based on stellar velocity dispersion  $\sigma_*$  via Tremaine et al. (2002), while the bolometric luminosity is calculated based on  $L_X$ , using the average bolometric correction of  $L_{\text{bol}}/L_X = 16$  (Ho 2008). There is a rather clear trend of spectral hardening with increasing accretion rate.  $\Gamma$  and  $L/L_{\text{edd}}$  are found to be negatively correlated.

Defining an accretion rate, i.e., calculating  $L/L_{\text{edd}}$ , for galaxies with  $L_X < 10^{42}$  erg s $^{-1}$  may be misleading if the X-ray emission in these objects is dominated by X-ray sources other than an accreting super massive BH (e.g., individual compact binaries or hot diffuse gas). Note however that the  $x$ -axis of Figure 6 is simply the measure of  $L_X/M_{\text{BH}}$  (or better,  $L_X/\sigma_*^4$ ), where both  $L_X$  and the BH mass  $M_{\text{BH}}$  (or  $\sigma_*$ ) are measured in exactly the same manner for all of the objects involved, and the trend remains even if this parameter is not interpreted as an accretion rate. The strongest likely dilution to accretion emission comes from contributions of the hot ISM in passive galaxies. Hot gas emission is soft, and relatively stronger in more massive hosts, both of which would push the passive galaxy points toward softer X-ray spectra (larger  $\Gamma$ ) and lower  $L_X/M_{\text{bh}}$ , which might spuriously accentuate the observed trend even in the absence of significant accretion power. Indeed, the observed trend is weakened once the passive galaxies are removed (Table 4). So while we rule out significant extended emission contributions in this sample, more detailed examination of such objects is warranted to determine the relative fractions of nuclear vs. extended hot gas contributions.

We measure the significance of the  $\Gamma - L/L_{\text{edd}}$  anti-correlation using the Spearman-rank test. The Spearman-rank coefficient, the chance probability, and the number of sources for each correlation are listed in Table 3. We fit the anti-correlation points with a linear least-squares method for the whole sample and for the subsamples of galaxies corresponding to different spectral types, using the `mpfit`<sup>10</sup> routine, being able to account for the errors in  $\Gamma$ . We show, for comparison, both the error weighted (continuous line) and the unweighted (dotted line) best-fits in Figure 6. The scatter around the best linear fit is large, and as expected the points with the largest error bars show the largest deviation. However, within the errors, the results of the fit remain unchanged when we use only objects with small measurements errors (i.e.,  $\Delta\Gamma/\Gamma < 50\%$ ). The results for the linear regression coefficients and the corresponding  $\chi^2$  and *dof* values are listed in Table 4. For the sake of considering “cleaner” AGN-like activity only, we also list here the results of such a fitting techniques to samples that exclude the Passive galaxies and the H IIs, and for samples of luminous X-ray systems ( $L_X \gtrsim 10^{42}$  erg s $^{-1}$ ) only, and indications of an anticorrelation, albeit weaker, remain.

The linear regression fits might appear at odds with the conclusion of the Spearman test, which indicates that  $\Gamma$  and  $L/L_{\text{edd}}$  are possibly anticorrelated for all the subsamples presented here. Note however that such a dis-

crepancy appears for the subsamples where the Spearman test remains rather inconclusive as, the probability that an anticorrelation appears by chance is large. Moreover, the Spearman test ignores the errors, and thus tests the unweighted data, for which linear regression fits are always consistent with negative slopes. It is clear however that for Seyferts in particular, there is no evidence for either positive or negative correlation between  $\Gamma$  and  $L/L_{\text{edd}}$ . This has been seen in other samples as well (Winter et al. 2009), and it is an important result. Nevertheless, investigations of the LLAGN phenomenon should not be restricted to these types of sources only.

In an attempt to provide some more physical insights into the reality and significance of this new trend, we also explore here the possible correlations between various X-ray measures that might influence (if not artificially create) it. In particular, we scrutinize the way our measured  $\Gamma$  relates to the number of counts, the X-ray flux and luminosity. Some studies showed that the photon index correlates with the X-ray luminosity, becoming softer in more luminous sources, whether measured in soft, 0.2 – 2 keV (Forster & Halpern 1996; Lu & Yu 1999; Gierlinski & Done 2004; Williams, Mathur, & Pogge 2004), or hard, 2 – 10 keV (Dai et al. 2004; Porquet et al. 2004; Wang, Watarai & Mineshige 2004) bands only, or comprising the whole spectrum, and even as they vary (Chiang et al. 2000; Petrucci et al. 2000; Vaughan et al. 2001). However, because many others have not found such trends, the idea that the choice of the sample involved in these studies may contribute to producing the correlations has also been put forward. Interestingly, our ChaMP sample does not show this correlation either. Figure 7 illustrates the dependence of  $\Gamma$  measured in the 0.5 – 8 keV range as a function of the total number of counts in this energy range, the X-ray flux, and the X-ray luminosity. As before, we emphasize the different optical spectral classifications; the fact that, e.g., the various types of galaxies separate rather well from each other in diagrams like this suggests that the correlation is physical, and most probably related to the accretion physics in these nuclei, rather than an artificial effect of fitting various (simple) models to their X-ray spectra.

#### 4.2. Comparison with high $z$ QSOs

The anti-correlation between  $\Gamma$  and  $L/L_{\text{edd}}$  (or simply,  $L_X/M_{\text{BH}}$ ) that we find to characterize the nuclear emission of nearby galaxies is certainly surprising. This trend is opposite to what more luminous galaxy nuclei, i.e., quasars, exhibit: their X-ray spectra soften as they become more luminous. Figure 8 shows the  $\Gamma - L/L_{\text{edd}}$  anti-correlation followed by the low luminosity galaxy nuclei along with measurements of  $\Gamma$  and  $L/L_{\text{edd}}$  for a sample of SDSS quasars with optical spectra that are ChaMP detected and X-ray analysed in the same manner we handled our sample of nearby galaxy nuclei (Green et al. 2009). The quasar  $L/L_{\text{edd}}$  values are obtained using the average bolometric correction of  $L/L_X = 83$  estimated by Ho (2008), with no luminosity-dependence, and the black hole masses from Shen et al. (2008).

To ease comparison with previous work on quasars, we use in this plot the 2 – 10 keV  $L_X$  luminosity, which is obtained by extrapolating the measured unobscured  $L_{0.5-8\text{keV}}$  value, using the best  $\Gamma$  measurements. Note

<sup>10</sup> <http://www.physics.wisc.edu/~craigm/idl/fitting.html>



that the anti-correlation between  $\Gamma$  and  $L/L_{\text{edd}}$  that nearby galaxy nuclei show is even more pronounced when the 2–10 keV  $L_X$  is plotted against  $\Gamma$ . This is expected, as softer objects will be less luminous in 2–10 keV than in the 0.5–8 keV range, while the hard objects will be more luminous. The magnitude of this effect, i.e., the ratio of the two  $L_X$  values is a function of the photon index  $\Gamma$ , as given by

$$L_X(2-10 \text{ keV}) = L_X(0.5-8 \text{ keV}) \times \frac{10^{2-\Gamma} - 2^{2-\Gamma}}{8^{2-\Gamma} - 0.5^{2-\Gamma}}. \quad (1)$$

The largest difference, and thus the most significant effect on the shape of the  $\Gamma - L/L_{\text{edd}}$  trend, is for the softest ( $\Gamma \gtrsim 3$ ) objects, however it does not exceed  $\sim 1$  dex. Note that for these particular objects the measurement errors are also among the highest, and hence contributed the least weight to the best-fit  $\Gamma - L/L_{\text{edd}}$  relation.

The ChaMP quasars fall well within the locus of values expected based on previous work. The ChaMP quasars do not show, however, a clear  $\Gamma - L/L_{\text{edd}}$  positive correlation. The ChaMP quasars span a wide range in redshift and their  $L/L_{\text{edd}}$  measurements reflect a mix of BH mass estimates based on all  $H\beta$ , Mg II, and C IV, which may add scatter to an underlying correlation (Shen et al. 2008). We show for comparison the results of linear regression fits of the  $\Gamma - L/L_{\text{edd}}$  correlation reported by Shemmer et al. (2008) and by Kelly et al. (2008), with the results for the  $H\beta$  and C IV based estimates of the  $M_{bh}$  shown separately. Note that we use here these data only for the purpose of global comparison of the quasar properties with those of the nearby galaxy nuclei, and do not attempt to improve upon the previous work on the characterization or calibration of the  $\Gamma - L/L_{\text{edd}}$  relation for quasars.

Clearly, the quasar  $\Gamma$ 's are not negatively correlated with their Eddington ratios, even with the shift in  $L_X$  produced by the energy conversion mentioned above, which might contribute to such trend (the quasar X-ray data is analysed and measured via the same techniques employed for the nearby galaxy nuclei). Thus, over the whole  $L/L_{\text{edd}}$  range we explore here by putting together luminous and weak AGN, there is clearly a break in the  $\Gamma - L/L_{\text{edd}}$  correlation, which seems to happen at  $L/L_{\text{edd}} \approx 10^{-2}$ , and  $\Gamma \gtrsim 1.5$ . It is important to note that, for the samples of quasars investigated by both Kelly et al. (2008) and Shemmer et al. (2008), the scatter in the claimed correlation between  $\Gamma$  and  $L/L_{\text{edd}}$  is largest as the samples reach the weakest accretion rates (while hardly reaching the  $L/L_{\text{edd}} \approx 10^{-2}$  level), and the hardest values ever measured for the quasar photon index  $\Gamma \gtrsim 1.5$ ; while suggestive of a break, the quasar data alone cannot however be used to single it out. Other studies that include measurements of lower luminosity managed to point out these types of deviations from the expected correlation (e.g., Zhang, Dultzin & Wang 2008; Green et al. 2009), however, the data remained sparse at those levels of accretion, leaving the effect unquantified.

We note here that the comparison of the nearby galaxies' central X-ray emission with that of the high redshift QSOs may be inadequate since X-rays from SF activity is not yet accounted for in the former.

We addressed this issue by including in the modelling of the original X-ray spectrum (Section 2.1) a  $\Gamma = 2$  component with the expected  $L_X(SF)$ . A power-law with  $\Gamma = 2$  provides the best simple description of the mix of hot gas and high mass X-ray binaries (HMXBs) that comprise the SF activity (e.g., Kim et al. 1992a,b; Nandra & Pounds 1994; Ptak et al. 1999; George et al. 2000; Colbert et al. 2004; Reddy & Steidel 2004; Lehmer, et al. 2005). To estimate the potential  $L_X(SF)$  in each galaxy, we use star-formation rates (SFR) calculated and available for these objects in the MPA/JHU catalog (Section 2; Brinchmann et al. 2004), along with the  $L_X - SFR$  correlation quantified by Gilvanov, Grimm, & Sunyaev (2004). There are 83 objects with total  $L_X$  above the line describing the  $L_X - SFR$  correlation, for which we modelled the remaining - presumably AGN component. This reanalysis produces significant deviations from the  $\Gamma - L_X/L_{\text{edd}}$  correlation only for 6% of the sample (5 out of the 83 objects involved in this analysis). The scatter and the error bars for both  $\Gamma$  and  $L_X$  are only slightly increased. The slope of the correlation flattens but remains consistent within the errors with our previous measurements.

#### 4.3. The “break” in the $\Gamma - L/L_{\text{edd}}$ correlation and comparison with XRBs

The X-ray photon index  $\Gamma$  and the Eddington ratio  $L/L_{\text{edd}}$  show a double-sloped relation, with positive and negative correlations above and below  $L/L_{\text{edd}} \approx 0.01$  and  $\Gamma \gtrsim 1.5$  respectively. We see now that, a given AGN spectral index  $\Gamma$  may correspond to two different luminosity levels, with the luminosity difference greater for sources characterized by softer spectra (Figure 8). This break in the  $\Gamma - L/L_{\text{edd}}$  relation, when studied over a large range of accretion power, fits well into the theoretical ideas of a transition in the AGN accretion mode: a standard (Shakura & Sunyaev 1973) accretion disk/corona at high Eddington rates, i.e., quasar phase, and an ADAF (e.g., Narayan & Yi 1994) at low  $L/L_{\text{edd}}$ . This break we find in the  $\Gamma - L/L_{\text{edd}}$  relation may provide the best empirical evidence to date for such a transition.

The inflection point in the  $\Gamma - L/L_{\text{edd}}$  relation is dominated by Ts, consistent with the optical nature of these systems. While hypothesized to be the result of mixed AGN and SF ionization (e.g., Ho, Filippenko, & Sargent 2003; Constantin et al. 2009), their AGN component could be either an S- or L-like. Ss appear to be the low  $L$  quasar-like, efficiently accreting systems, while the Ls are the ADAF objects, so T's locus at the break region is suggestive of a switch in the accretion mode. The optically-defined Ts are then transition systems that map the X-ray inflection as well.

Note that this idea of transition in the accretion mode, from ADAF to standard-disk as the accretion rates increases, has been first proposed, and later developed, mainly based on results of investigations of smaller BH mass accretors, i.e., stellar mass black-hole X-ray binaries, or XRBs; see Narayan & McClintock (2008) for a recent review. Interestingly, the relation between  $\Gamma$  and  $L/L_{\text{edd}}$  that XRBs exhibit in the different phases of their temporal variability is also multivalued: a given spectral index  $\Gamma$  may correspond to two different lumi-

osity levels, with the luminosity difference greater for sources characterized by softer spectra. That is, the XRBs show a positive  $\Gamma - L/L_{\text{edd}}$  correlation while in their high/soft states (e.g., Kubota & Makishima 2004), and an anti-correlation while in their low/hard states (e.g., Yamaoka et al. 2005). Several clear examples of such a turn (or convergence point) in the  $\Gamma - L/L_{\text{edd}}$  relation measured in XRBs are illustrated in, e.g., Yuan et al. (2007) and Wu & Gu (2008).

In terms of the physical phenomenology governing the black hole accretion process over more than 10 orders of magnitude in the Eddington ratio, the transition from an ADAF to a standard disk accretion seems to adequately account for both the XRB and AGN emission properties. The ADAF scenario qualitatively explains the anti-correlation via Comptonization of thermal synchrotron photons as the dominant cooling mechanism at low  $L/L_{\text{edd}}$  ratios: the Compton  $y$ -parameter increases with increasing of the optical depth, which is caused by increase of the accretion rate, the X-ray spectrum becomes harder (Esin et al. 1997). Further increase in the accretion rate would cause both an increase in the released energy and a decrease in the electron temperature, weakening the corona, and consequently the optical depth, reducing the  $y$ -parameter, and leading to softer spectra, and thus the positive  $\Gamma - L/L_{\text{edd}}$  correlation (e.g., Janiuk & Czerny 2000). The ADAF scenario has been relatively successful in explaining a variety of the LLAGN properties (Ho 2008), while the standard disk-corona model has been widely invoked to explain quasar emission. Our finding of a non-monotonic  $\Gamma - L/L_{\text{edd}}$  relation seems to provide the first direct empirical link between these two different types of accretion in AGN.

The AGN-XRB physical analogy has been discussed rather extensively (see Maccarone, Fender & Ho 2005), and is particularly supported by the two "fundamental planes" of the BH activity on all mass scales, the  $L_{\text{radio}} - L_X - M_{bh}$  (Merloni, Heinz & di Matteo 2003; Falcke, K rding & Markoff 2004) and the  $L_{\text{bol}} - M_{bh} - T_{\text{break}}$  (McHardy et al. 2006). There was however not much evidence for existence of spectral states in massive black holes, similar to those of the stellar black holes. Our discovery of an anti-correlation between  $\Gamma$  and  $L/L_{\text{edd}}$ , and thus the discovery of a turning point in the  $\Gamma - L/L_{\text{edd}}$  relation for AGN, provides this evidence, which constitutes an important empirical constraint to the idea that these systems are really the analogs of each other, in spite of the vast difference of scales.

## 5. CONCLUSIONS & DISCUSSION

This study of serendipitous Chandra nearby sources brings together for the first time a large homogeneous sample of active and inactive galaxy nuclei selected and classified based on their optical spectral properties. With a minimal selection bias, we characterize the X-ray properties of low luminosity AGN via measurements of the X-ray spectral shape, fluxes, and luminosities. These measurements add important information and provide new constraints to the proposed  $H II \rightarrow S/T \rightarrow L \rightarrow P$  galaxy evolutionary sequence. Optical observations reveal that at least in statistical terms, along this sequence, (1) the host halo mass increases, (2) the environmental density increases, (3) both central BH mass and stellar mass increase, while (4) the rate of accretion onto the central

Bh decreases, (5) the stellar population ages, and (6) the material that could be used for accretion and/or star-formation is less and less available. The X-ray data support these evolutionary trends and bring surprising new insights into the nature of the LLAGN phenomenon.

There are two main results of this analysis that we want to emphasize here:

- The  $(H II \rightarrow) \text{ Seyfert} \rightarrow \text{Transition Object} \rightarrow \text{LINER} \rightarrow \text{Passive Galaxy}$  sequence suggested by a large variety of optical measures is supported by X-ray measurements. Both the spectral shape and the accretion power, as measured by  $L_X$  and the Eddington ratio  $L/L_{\text{edd}}$ , with  $L = L_{\text{bol}} = 16 \times L_X$ , show a clear trend toward softer, less X-ray luminous and less actively accreting sources from  $S$ s to  $T$ s, to  $L$ s, and, at the end, the *Passive* galaxies. The rather ambiguous (in some optical properties) succession of  $S$  and  $T$  phases is now significantly constrained by the X-ray activity to follow in a sense of decreasing accretion power.
- There is a rather strong anti-correlation between the shape of the X-ray spectral energy distribution, quantified via the power-law index  $\Gamma$ , and  $L/L_{\text{edd}}$ . This finding translates into a break in the  $\Gamma - L/L_{\text{edd}}$  correlation exhibited by AGN of all powers, with spectral softening on either side of  $L/L_{\text{edd}} \approx 0.01$ . The transition point is identical to that where stellar mass BH accretors (XRBs) exhibit their turn in analogous  $\Gamma - L/L_{\text{edd}}$  trends.

The distribution of points within the observed  $\Gamma - L/L_{\text{edd}}$  relation exhibited by both weak and powerful AGN might have other implications as well. The presence of some LLAGN below the  $\Gamma \lesssim 1.5$  turning point, which are mostly Seyferts, suggests that obscuration might also play a role in shaping the observed  $\Gamma - L/L_{\text{edd}}$  trends at low and high  $z$ . These particular objects' rather hard photon indices must be the indication of gas absorption of their 0.5 – 8 keV spectra. Their Eddington ratios huddle near the  $10^{-2}$  level, being generally weak when compared to the luminous quasars, and among the strongest LLAGN. Thus, the anti-correlation between  $\Gamma$  and  $L/L_{\text{edd}}$  shown by the nearby galaxy nuclei may well be interpreted as a relation between absorption and accretion rate, the objects accreting at higher rates being more obscured.

The probably naive extrapolation of this idea at higher  $L/L_{\text{edd}}$  suggests then that more active AGN are also more absorbed. Consequently, these increasingly absorbed systems, that would be the type 2 ones [according to the AGN "unification" scenario that separates (the observed appearance of) AGN in terms of orientation relative to the line of sight] would be decreasingly likely to be included in the (current) optically selected AGN/quasar samples. This interpretation is certainly consistent with the general results of various quests for type 2 quasars: their X-ray spectra are harder than their type 1 counterparts (Zakamska et al. 2004; Ptak et al. 2006), and they are highly obscured (Zakamska et al. 2005). The type 2 quasars are definitely scarce compared with the type 1, and their fraction relative to that of the type 1 ones decreases with increasing luminosity (Reyes et al.

2008). Thus, this may as well be the explanation for the dearth of type 2 quasars.

If the type 1-2 dichotomy and consequently the "unification" are only about the observing angle, the AGN-galaxy evolutionary sequence suggested by the properties of the different types of nearby galactic nuclei should be even stronger once inclination effects are removed, as we would have a clearer view of the central engine. On the other hand, the 1-2 type separation, and thus the unification, might be the result of evolution. Some simulations suggest that for the luminous quasars, the type 1 (unobscured) phase comes after a phase of "blowing-out" circumnuclear matter, which might mean after the quasars were observable as type 2. By adding type 1 LLAGN to investigations of the  $\Gamma - L/L_{\text{edd}}$  connection we might be able to understand better the way the proposed evolutionary sequence does or does not challenge the unification scenario.

Also, the exact location of the turning point in the  $\Gamma - L/L_{\text{edd}}$  relation remains to be better quantified in terms of both parameters. Of particular caution is combining the  $L/L_{\text{edd}}$  measurements of LLAGN with those of quasars, mainly because the methods used in estimating their BH masses are not necessarily compatible. The BH masses of LLAGN are based on the  $M_{\text{bh}} - \sigma_*$  relation, while the (usually high  $z$ ) quasar BH masses are obtained from the widths of the optical broad emission lines via scaling relations; the scaling relations are calibrated on  $M_{\text{bh}} - \sigma_*$ , which, recent work suggests, does not necessarily hold at high  $z$ . Another way of refining the exact location of the break lies of course in better estimates of  $\Gamma$ , i.e., higher quality (higher signal-to-noise) X-ray measurements, and/or larger samples. The latter

alternative, in particular, seems to be feasible, as larger and larger samples of well characterized samples of optically selected AGN become available for cross-correlation with X-ray detections from, e.g., serendipitous surveys like ChaMP.

Future work (Constantin & ChaMP 2009, in prep.) will explore the multi-wavelength properties of a large sample of AGN that brings together nearby LLAGN of type 2 with nearby quasars (type 1 AGN), thus attempting to reconcile both the type 1-2 dichotomy and the problem of mix-matching BH masses, along with providing larger statistics, and better means of quantifying extrinsic effects such as absorption and non-thermal processes (i.e., Comptonized emission from the accretion disk's corona) that enable improved constraints to the analogy with XRBs. We will also address in this work the biases that are potentially present in the previously claimed relationships between the between  $L_X$  and optical emission line luminosities for LLAGN, together with the impact of using optical emission lines to estimate  $L_{\text{bol}}$ , and thus to the overall shape of the  $\Gamma - L/L_{\text{edd}}$  relation.

AC thanks Christy Tremonti for valuable discussions regarding the MPA/JHU catalog. Support for this work was provided by the National Aeronautics and Space Administration through *Chandra* Award Number AR7-8015A issued by the *Chandra* X-ray Observatory Center, which is operated by the Smithsonian Astrophysical Observatory for and on behalf of the National Aeronautics Space Administration under contract NAS8-03060.

## REFERENCES

- Aldcroft, T.L. 2006, *Bulletin of the American Astronomical Society*, 38, 376
- Baldwin, J. A. Phillips, M. M. & Terlevich, R., 1981, *PASP*, 93, 5
- Barkhouse, W., et al., 2006, *ApJ*, 645, 955
- Barth, A., & Shields, C. J., 2000, *PASP*, 112, 753
- Blandford, R.D., & Begelman, M.C., 1999, *MNRAS*, 303, 1
- Bohringer, H., et al. 2001, *A&A*, 365, 181
- Brinchmann, J., Charlot, S., Heckman, T. M., Kauffmann, G., Tremonti, C., & White, S.D.M., 2004, *astro-ph/0406220*
- Brinchmann, J., Charlot, S., White, S.D.M., Tremonti, C., Kauffmann, G., Heckman, T. M., & Brinkmann, J., 2004, *MNRAS*, 351, 1151
- Cappi, M., et al., 2006, *A&A*, 446, 459
- Cash, W. 1979, *ApJ*, 228, 939
- Charlot, S., & Fall, S. M., *ApJ*, 539, 718
- Chiang, J., Reynolds, C. S., Blaes, O. M., Nowak, M. A., Murray, N., Madejski, G., Marshall, H. L., & Magdziarz, P., 2000, *ApJ*, 528, 292
- Cid Fernandes, R., Gonzalez Delgado, R. M., Storchi-Bergmann, T., Martins, L.P., & Schmitt, H., 2005, *MNRAS*, 356, 270
- Colbert, E. J. M., Heckman, T. M., Ptak, A. F., Strickland, D. K., & Weaver, K. A., 2004, *ApJ*, 602, 231
- Constantin, A., & Vogeley, M.S., 2006, *ApJ*, 650, 727
- Constantin, A., Hoyle, F., & Vogeley, M.S., 2008, *ApJ*, 673, 715
- Constantin, A., Shields, J.C., Ho, L.C., Barth, A., and Filippenko, A.V., 2009, in preparation.
- Cowie, L. L. & Barger, A. J., 2008, *ApJ*, 686, 72
- Czerny, B., Nikolajuk, M., Raska, A., Dumont, A.-M., Loska, Z., Zycki, P. T., et al. 2003, *A&A*, 412, 317
- Dai, X., Chartas, G., Eracleous, M., Garmire, G.P., 2004, *ApJ*, 605, 45
- Dickey, J.M., & Lockman, F.J., 1990, *ARA&A*, 28, 215
- Dudik, R. P., Satyapal, S., Gliozzi, M., & Sambruna, R. M., 2005, *ApJ*, 620, 620, 113
- Esin, A.A., McClintock, J.E., & Narayan, R., 1997, *ApJ*, 489, 865
- Eracleous, M., Shields, J. C., Chartas, G., & Moran, E. C., 2002, *ApJ*, 565, 108
- Falcke, H, K rding, E., & Markoff, S., 2004, *A&A*, 414, 895
- Filho, M. E., Fraternali, F., Markoff, S., Nagar, N. M., Barthel, P. D., Ho, L. C., & Yuan, F., 2004, *A&A*, 418, 429
- Filippenko, A. V., & Terlevich, R., 1992, *ApJ*, 397, 79
- Flohic, H.M.L.G., Eracleous, M., Chartas, G., Shields, J.C., & Moran, E.C., 2006, *ApJ*, 647, 140
- Forster, K. & Halpern, J.P., 1996, *ApJ*, 468, 565
- Georgantopoulos, I., Panessa, F., Akylas, A., Zezas, A., Cappi, M., & Comastri, A., 2002, *A&A*, 386, 60
- George, I.M. & Fabian A.C., 1991, *MNRAS*, 249, 352
- George, I. M., Turner, T. J., Yaqoob, T., Netzer, H., Laor, A., Mushotzky, R. F., Nandra, K., & Takahashi, T., 2000, *ApJ*, 531, 52
- Gierlinski, M. & Done, C., 2004, *MNRAS*, 349, 7
- Gonzalez-Martin, O., Masegosa, J., Marquez, I., Guerrero, M. A., & Dultzin-Hacyan, D., 2006, *A&A*, 460, 45
- Green, P. J., et al., 2004, *ApJS*, 150, 43
- Green, J.P., et al., 2009, *ApJ*, 690, 644
- Greene, J.E., & Ho, L.C., 2007, *ApJ*, 656, 84
- Haardt, F. & Maraschi, L., 1991, *ApJ*, 380, 51
- Halderson, E.L., Moran, E.C., Filippenko, A.V., & Ho, L.C., 2001, *AJ*, 122, 637
- Heckman, T. M., Kauffmann, G., Brinchmann, J., Charlot, S., Tremonti, C., White, S. D. M., 2004, *ApJ*, 613, 109
- Ho, L. C., Filippenko, A. V., & Sargent, W. L. W., 1993, *ApJ*, 417, 63
- Ho, L. C., Filippenko, A. V., & Sargent, W. L. W., 1997a, *ApJS*, 112, 315
- Ho, L. C., Filippenko, A. V., & Sargent, W. L. W., 1997b, *ApJ*, 487, 568

- Ho, L. C., Feigelson, E., D., Townsley, L. K., Sambruna, R. M., Garmire, G. P., Brandt, W. N., Filippenko, A. V., Griffiths, R. E., Ptak, A. F., & Sargent, W. L. W. 2001, *ApJ*, 549, L51
- Ho, L. C., Filippenko, A. V., & Sargent, W. L. W., 2003, *ApJ*, 583, 159
- Ho, L. C., 2008, *ARA&A*, 46, 475
- Hopkins, P.F., & Hernquist, L., 2006, *ApJ*, 166, 1
- Hopkins, P.F., & Hernquist, L., 2009, *ApJ*, in press (arXiv0809.3789)
- Ishisaki, Y., et al., 1996, *PASJ*, 48, 237
- Iyomoto, N., Makishima, K., Matsushita, K., Fukazawa, Y., Tashiro, M., & Ohashi, T., 1998, *ApJ*, 503, 168
- Iyomoto, N., Fukazawa, Y., Nakai, N., & Ishihara, Y., 2001, *ApJ*, 561, 69
- Janiuk, A., & Czerny, B., 2000, *NewA*, 5, 7
- Kalemci, E., Tomsick, J. A., Buxton, M. M., Rothschild, R. E., Pottschmidt, K., Corbel, S., Brocksopp, C., & Kaaret, P., *ApJ*, 622, 508
- Kauffmann, G., et al., 2003, *MNRAS*, 341, 33
- Kauffmann, G., et al., 2003, *MNRAS*, 346, 105
- Kauffmann, G., et al., 2004, *MNRAS*, 353, 713
- Kauffmann, G., & Heckman, T.M., 2009, *MNRAS*, submitted (arXiv0812.1224)
- Kelly, B. C., Bechtold, J., Trump, J. R., Vestergaard, M., & Siemiginowska, A., 2008, *ApJ*, 176, 355
- Kewley, L., Dopita, M. A., Sutherland, R. S., Heisler, C. A., & Trevena, J., 2001, *ApJ*, 556, 121
- Kewley, L.J., Groves, B., Kauffmann, G., & Heckman, T., 2006, *MNRAS*, 372, 961
- Kim, D.-W., Fabbiano, G., & Trinchieri, G., 1992, *ApJ*, 393, 134
- Kim, D.-W., Fabbiano, G., & Trinchieri, G., 1992, *ApJS*, 80, 645
- Kim, D.-W. & Fabbiano, G., 2003, *ApJ*, 586, 826
- Kollmeier, J.A., et al., 2006, *ApJ*, 648, 128
- Kubota, A., & Makishima, K., 2004, *ApJ*, 601, 428
- Lehmer, B., et al. 2005, *ApJ*, 129, 1
- Lightman, A.P. & White, T.R., 1988, *ApJ*, 335, 57
- Lu, Y. & Yu, Q., 1999, *ApJ*, 526, 5
- Lu, J.-F., Li, S.-L., Gu, W.-M., 2004, *MNRAS*, 352, 147
- Maccarone, T.J., Fender, R.P., & Ho, L.C., 2005, *From X-ray Binaries to Quasars: Black Hole Accretion on All Mass Scales* Dordrecht:Luwer,
- McHardy, I. M., Koerding, E., Knigge, C., Uttley, P., Fender, R. P., 2006, *Nature*, 444, 730
- McLure, R.J., & Dunlop, J.S., 2004, *MNRAS*, 352, 1390
- Merloni, A., Heinz, S., di Matteo, T., 2003, *MNRAS*, 345, 1057
- Miniutti, G., Ponti, G., Greene, J. E., Ho, L. C., Fabian, A. C., Iwasawa, K., 2008, *MNRAS*, 394, 443
- Nandra, K. & Pounds, K.A., 1994, *MNRAS*, 268, 405
- Narayan, R., & Yi, I., 1994, *ApJ*, 428, 13
- Narayan, R., Igomenshchev, & I. V., Abramowicz, M. A., 2000, *ApJ*, 539, 798
- Narayan, R., & McClintock, J.E., 2008, *New Astronomy Reviews*, 51, 733
- Nayakshin, S., 2000, *ApJ*, 540, 37
- Netzer, H., Lira, P., Trakhtenbrot, B., Shemmer, Ohad, & Cury, I., 2007, *ApJ*, 671, 1256
- Osterbrock, D. E., 1989, *Astrophysics of Gaseous Nebulae and Active Galactic Nuclei*, University Science Books
- Page, M. J., Soria, R., Zane, S., Wu, K., & Starling, R. L. C., 2004, *A&A*, 422, 77
- Panessa, F., Bassani, L., Cappi, M., Dadina, M., Barcons, X., Carrera, F. J., Ho, L. C., & Iwasawa, K., L., 2006, *A&A*, 455, 173
- Parejko, J. K., Constantin, A., Vogeley, M. S., & Hoyle, F., 2008, *AJ*, 135, 10
- Pellegrini, S., Cappi, M., Bassani, L., Malaguti, G., Palumbo, G. G. C., & Persic, M., 2000a, *A&A*, 353, 447
- Pellegrini, S., Cappi, M., Bassani, L., della Ceca, R., & Palumbo, G. G. C., 2000b, *A&A*, 360, 878
- Pellegrini, S., Fabbiano, G., Fiore, F., Trinchieri, G., & Antonelli, A., 2002, *A&A*, 383, 1
- Pellegrini, S., Baldi, A., Fabbiano, G., & Kim, D.-W., 2003, *ApJ*, 597, 175
- Pellegrini, S., 2005, *ApJ*, 624, 155
- Petrucci, P. O., Haardt, F., Maraschi, L., Grandi, P., Matt, G., Nicastro, F., Piro, L., Perola, G. C., & De Rosa, A., 2000, *ApJ*, 540, 131
- Porquet, D., Reeves, J. N., O'Brien, P., & Brinkmann, W., *A&A*, 422, 85
- Poutanen, J., Krolik, J. H., Ryde, F., 1997, *MNRAS*, 292, 21
- Proga, D., 2005, *ApJ*, 630, 9
- Ptak, A., Yaqoob, T., Serlemitsos, P. J., Kunieda, H., & Terashima, Y., 1996, *ApJ*, 459, 542
- Ptak, A., Serlemitsos, P., Yaqoob, T., & Mushotzky, 1999, *ApJS*, 120, 179
- Ptak, A., Terashima, Y., Ho, L. C., Quataert, E., 2004, *ApJ*, 606, 173
- Ptak, A., Zakamska, N. L., Strauss, M. A., Krolik, J. H., Heckman, T. M., Schneider, D. P., & Brinkmann, J., 2006, *ApJ*, 637, 147
- Reddy, N.A., & Steidel, C.C., 2004, *ApJ*, 603, 13
- Reyes, R., Zakamska, N. L., Strauss, M. A., Green, J., Krolik, J. H., Shen, Y., Richards, G. T., Anderson, S. F., Schneider, D. P., 2008, *AJ*, 136, 2373
- Roberts, T. P., Warwick, R. S., 2000, *MNRAS*, 315, 98
- Roberts, T. P., Schurch, N. J., Warwick, R. S., 2001, *MNRAS*, 324, 737
- Satyapal, S., Sambruna, R. M., & Dudik, R. P., 2004, *A&A*, 414, 825
- Satyapal, S., Dudik, R. P., O'Halloran, B., Gliozzi, M., 2005, *ApJ*, 633, 86
- Shakura, N. I., & Syunyaev, R. A., 1973, *A&A*, 24, 337
- Shapiro, S. L., Lightman, A. P., & Eardley, D. M., 1976, *ApJ*, 204, 187
- Shemmer, O., Brandt, W. N., Netzer, H., Maiolino, R., & Kaspi, S., 2008, *ApJ*, 682, 81
- Shen, Y., Greene, J. E., Strauss, M. A., Richards, G.T., Schneider, D.P., 2008, *ApJ*, 680, 169
- Shields, J. C., 1992, *ApJ*, 399, 27L
- Sobolewska, M.A., Siemiginowska, A., & ycki, P.T., 2004, *ApJ*, 617, 102
- Soria, R., Fabbiano, G., Graham, A.W., Baldi, A., Elvis, M., Jerjen, H., Pellegrini, S., & Siemiginowska, A., 2006, *ApJ*, 640, 126
- Starling, R. L. C., Page, M. J., Branduardi-Raymont, G., Breeveld, A. A., Soria, R., & Wu, K., 2005, *MNRAS*, 356, 727
- Stasiska, G., Asari, N.V., Fernandes, R.C., Gomes, J.M., Schlickmann, M., Mateus, A., Schoenell, W., & Sodr, L., Jr., 2008, *MNRAS*, 391, 29
- Taniguchi, Y., Shioya, Y., & Murayama, T., 2000, *AJ*, 120, 1265
- Terashima, Y., et al., 1998
- Terashima, Y., Ho, L.C., Ptak, A.F., 2000a, *ApJ*, 539, 161
- Terashima, Y., Ho, L.C., Ptak, A.F., Mushotzky, R. F., Serlemitsos, P. J., Yaqoob, T., Kunieda, H., 2000b, *ApJ*, 533, 729
- Terashima, Y., Iyomoto, N., Ho, Luis C., Ptak, A.F., 2002, *ApJS*, 139, 1
- Terashima, Y., & Wilson, A. S., 2003, *ApJ*, 583, 145
- Tremaine, S., et al., 2002, *ApJ*, 574, 740
- Tremonti, C.A., et al., 2004, *ApJ*, 613, 898
- Veilleux, S., & Osterbrock, D. E., 1987, *ApJS*, 63, 295
- Vignali, C., Brandt, W. N., Schneider, D. P., Kaspi, S., 2005, *AJ*, 129, 2519
- Vaughan, S., Edelson, R., Warwick, R. S., Malkan, M. A., & Goad, M. R., 2001, *MNRAS*, 327, 673
- Wang, J.-M., Watarai, K.-Y., & Mineshige, S., 2004, *ApJ*, 607, 107
- Williams, R. J., Mathur, S., & Pogge, R.W., 2004, *ApJ*, 610, 737
- Winter, L. M., Mushotzky, R. F., Reynolds, C. S., Tueller, J., 2009, *ApJ*, 690, 1322
- Wu, Q., & Gu, M., 2008, *ApJ*, 682, 212
- Yaqoob, T., Edelson, R., Weaver, K. A., Warwick, R. S., Mushotzky, R. F., Serlemitsos, P. J., Holt, S. S., 1995, *ApJ*, 453, 81
- Yamaoka, K., Uzawa, M., Arai, M., Yamazaki, T., & Yoshida, A., 2005, *ChJAS*, 5, 273
- Yu, Q., & Tremaine, S., 2002, *MNRAS*, 335, 965
- Yuan, F. & Narayan, R., 2004, *ApJ*, 612, 724
- Yuan, F., Taam, R. E., Misra, R., Wu, X.-B., & Xue, Y., 2007, *ApJ*, 658, 282
- Zakamska, N. L., Strauss, M. A., Heckman, T. M.; Ivezi, ., Krolik, J. H., 2004, *AJ*, 128, 1002

Zakamska, N. L., Schmidt, G. D., Smith, P. S., Strauss, M. A.,  
Krolik, J. H., Hall, P. B., Richards, G. T., Schneider, D. P.,  
Brinkmann, J., Szokoly, G. P., 2005, AJ, 129, 1212  
Zdziarski, A. A., Lubinski, P., Smith, David A., 1999, MNRAS,  
303, 11

Zhang, X.-G., Dultzin, D., & Wang, T.-G., 2008, MNRAS, 385,  
1087

TABLE 1  
X-RAY MEASUREMENTS OF CHAMP-SDSS GALAXIES

ObjID (1)	ra (2)	dec (3)	z (4)	srcid (5)	OAA (6)	counts (7)	Exp. (8)	Targ. (9)	$N_H^{Gal}$ (10)	$N_H^{Intr.}$ (11)	$\Gamma$ (12)	$f_x$ (13)	$L_X$ (14)	Opt. Class (15)
587722982300254964	233.296661	-0.756684	0.151	CXOMP J153311.1-004524	6.8	27.6	4.9	...	6.39	$6.9^{+3.6}_{-2.4}$	$-0.7^{+0.5}_{-0.6}$	218.41	42.94	S
587722983362134277	206.118027	0.029700	0.135	CXOMP J134428.3+000146	2.4	5.7	8.7	...	1.93	$\text{j}0.8$	$2.1^{+1.3}_{-1.1}$	5.14	41.06	P
587722984431026387	195.126404	1.046143	0.067	CXOMP J130030.3+010246	8.4	16.6	1.5	...	1.63	$\text{j}1.3$	$1.3^{+0.6}_{-0.6}$	152.65	42.05	T
587725041163370794	174.768066	-1.980904	0.342	CXOMP J113904.3-015851	3.5	2.5	14.0	...	2.56	$\text{j}0.4$	$4.3^{+5.1}_{-2.5}$	1.03	40.50	P
587725470127161548	118.935455	41.204029	0.074	CXOMP J075544.5+411214	10.1	33.9	7.2	...	4.62	$\text{j}0.0$	$3.0^{+0.7}_{-0.6}$	50.35	41.14	P
587725550133117038	155.188263	63.196468	0.206	CXOMP J102045.1+631147	4.2	39.8	6.0	...	1.03	$\text{j}0.0$	$2.4^{+0.5}_{-0.4}$	51.62	42.38	T
587725550136983727	174.983627	66.098259	0.376	CXOMP J113956.0+660553	5.6	15.0	114.6	...	1.17	$\text{j}0.3$	$2.8^{+1.0}_{-0.8}$	0.99	41.19	P
587725551735996593	127.912956	52.701363	0.058	CXOMP J083139.1+524204	3.7	23.5	6.8	...	3.91	$\text{j}1.4$	$-0.4^{+0.5}_{-0.6}$	87.79	41.77	S
587725591458414903	264.505035	58.503334	0.330	CXOMP J173801.2+583012	3.3	138.8	4.5	...	3.56	$\text{j}0.1$	$1.8^{+0.4}_{-0.4}$	192.16	43.55	T
587725980689301524	128.116867	52.605656	0.016	CXOMP J083228.0+523620	11.6	41.7	9.0	...	3.84	$\text{j}0.0$	$2.9^{+0.6}_{-0.5}$	45.71	39.77	H II
587726015607275687	183.399002	2.810350	0.132	CXOMP J121335.7+024837	2.2	11.4	18.0	...	1.75	$\text{j}0.8$	$1.6^{+0.8}_{-0.8}$	7.37	41.31	L
587726015607275717	183.441772	2.811480	0.073	CXOMP J121346.0+024841	4.2	10.4	18.6	...	1.75	$\text{j}0.6$	$2.0^{+1.0}_{-0.9}$	13.05	40.90	T
587726031729459313	220.677521	1.319711	0.033	CXOMP J144242.6+011910	8.1	119.7	10.9	...	3.35	$\text{j}0.2$	$1.6^{+0.7}_{-0.5}$	106.12	41.22	L
587726033305338033	141.248947	2.241570	0.148	CXOMP J092459.7+021429	4.4	7.3	17.1	...	3.73	$\text{j}3.2$	$0.5^{+0.9}_{-1.0}$	8.14	41.53	no-class
587726100949238048	219.718658	3.716406	0.291	CXOMP J143852.4+034259	9.0	22.6	54.6	...	2.63	$\text{j}0.1$	$3.7^{+1.1}_{-0.9}$	5.71	41.28	P
587727179536138389	30.007231	-8.927990	0.052	CXOMP J020001.7-085540	4.8	29.9	34.2	...	2.09	$\text{j}0.2$	$2.0^{+0.6}_{-0.5}$	8.64	40.43	S
587727213347209620	322.206177	-7.787057	0.070	CXOMP J212849.4-074713	10.1	12.7	19.5	...	4.88	$21.6^{+51.2}_{-9.1}$	$-1.3^{+1.4}_{-2.5}$	28.58	41.43	H II
587727223009510128	325.644348	12.505494	0.276	CXOMP J214234.6+123019	2.6	5.0	14.0	...	6.69	$\text{j}1.3$	$2.0^{+1.3}_{-1.1}$	2.70	41.49	P
587727227305394267	10.728508	-9.230717	0.076	CXOMP J004254.8-091350	7.3	13.4	9.6	...	3.53	$\text{j}0.1$	$4.0^{+1.2}_{-1.0}$	19.63	40.24	L
587727227305394310	10.752554	-9.229577	0.076	CXOMP J004300.6-091346	7.7	63.5	9.6	...	3.54	$\text{j}0.1$	$2.5^{+0.4}_{-0.4}$	69.02	41.50	L
587727884161581244	29.994183	-8.826961	0.392	CXOMP J015958.6-084937	2.1	19.3	34.8	...	2.11	$\text{j}2.1$	$1.3^{+0.6}_{-0.6}$	7.32	42.35	H II
587727884161581256	29.955580	-8.833209	0.405	CXOMP J015949.3-084959	1.6	917.4	34.8	I	2.10	$\text{j}0.2$	$1.9^{+0.1}_{-0.1}$	254.49	43.88	no-class
587727942420988082	144.690018	0.990713	0.171	CXOMP J093845.6+005926	1.7	16.9	1.2	...	4.22	$\text{j}0.4$	$1.4^{+0.6}_{-0.6}$	114.19	42.76	T
587728307491897590	168.966110	1.498703	0.352	CXOMP J111551.8+012955	2.1	286.1	15.1	I	4.37	$\text{j}0.2$	$2.1^{+0.3}_{-0.2}$	168.98	43.52	T
587728905564258619	120.236748	36.056530	0.287	CXOMP J080056.8+360323	1.3	496.6	35.4	I	4.95	$0.1^{+0.1}_{-0.1}$	$2.0^{+0.3}_{-0.3}$	90.87	43.10	no-class
587729157893456002	196.494354	3.956814	0.023	CXOMP J130558.6+035724	3.0	55.1	112.0	...	2.08	$\text{j}0.1$	$1.3^{+0.4}_{-0.3}$	4.26	39.56	T
587729157893456055	196.563110	3.931599	0.110	CXOMP J130615.1+035553	1.6	16.8	112.0	...	2.08	$\text{j}0.1$	$2.5^{+1.0}_{-0.8}$	0.76	39.91	T
587729158440419656	219.591049	3.670265	0.224	CXOMP J143821.8+034012	3.6	37.0	56.2	I	2.61	$\text{j}0.4$	$1.9^{+0.5}_{-0.5}$	7.36	41.74	no-class
587729158440419712	219.609650	3.649648	0.235	CXOMP J143826.3+033858	2.3	19.6	56.2	...	2.61	$\text{j}0.1$	$3.8^{+1.0}_{-0.9}$	3.42	40.79	P
587729388215337158	139.517227	51.687130	0.186	CXOMP J091804.1+514113	6.2	23.4	18.7	...	1.48	$12.1^{+7.3}_{-5.3}$	$-0.6^{+0.6}_{-0.7}$	43.52	42.41	T
587729751132667997	247.652924	40.131489	0.077	CXOMP J163036.7+400753	4.2	10.8	26.0	...	0.88	$\text{j}0.1$	$3.4^{+1.2}_{-1.0}$	3.53	39.86	T
587729751132668135	247.629547	40.156597	0.077	CXOMP J163031.0+400923	2.7	20.6	24.8	...	0.88	$\text{j}0.1$	$3.4^{+1.0}_{-0.9}$	3.56	39.83	T
587729752213815608	260.041504	26.625124	0.159	CXOMP J172009.9+263730	2.2	566.4	24.0	I	3.89	$\text{j}0.2$	$2.1^{+0.3}_{-0.2}$	209.66	42.84	T
587729753280741824	250.473267	40.029160	0.466	CXOMP J164153.5+400144	2.5	23.4	45.3	I	1.02	$\text{j}0.3$	$2.3^{+0.8}_{-0.6}$	4.84	42.24	no-class
587730816826671317	340.846375	-9.518315	0.144	CXOMP J224323.1-093105	6.4	32.9	18.2	...	4.33	$3.0^{+1.6}_{-1.1}$	$0.1^{+0.4}_{-0.5}$	45.66	42.25	S
587731185129816192	359.235931	-0.986925	0.032	CXOMP J235656.6-005912	1.2	9.2	17.9	...	3.52	$\text{j}0.3$	$2.1^{+1.3}_{-0.9}$	4.77	39.73	L
587731186729550057	334.344727	0.351939	0.095	CXOMP J221722.7+002106	6.1	14.6	75.4	...	4.61	$\text{j}0.5$	$1.5^{+0.8}_{-0.7}$	2.23	40.51	T
587731187277430877	359.432159	0.654831	0.023	CXOMP J235743.7+003917	7.4	147.9	11.9	...	3.32	$1.7^{+0.6}_{-0.5}$	$0.9^{+0.2}_{-0.2}$	438.43	41.62	S
587731187277430877	359.431946	0.655582	0.023	CXOMP J235743.6+003920	7.4	142.7	11.9	...	3.32	$1.9^{+0.7}_{-0.6}$	$0.5^{+0.3}_{-0.3}$	525.45	41.73	S
587731187813253146	357.074768	1.104287	0.092	CXOMP J234817.9+010615	7.7	36.5	48.7	...	3.96	$\text{j}0.04$	$3.4^{+0.7}_{-0.6}$	6.36	40.25	P
587731511532453955	19.723360	-1.002003	0.045	CXOMP J011853.6-010007	1.7	217.6	38.3	I	3.67	$0.7^{+0.4}_{-0.3}$	$5.7^{+2.0}_{-1.5}$	28.49	40.62	no-class
587731512613404741	36.155399	-0.047232	0.127	CXOMP J022437.2-000250	0.8	12.0	86.7	...	2.85	$\text{j}0.6$	$1.7^{+0.9}_{-0.7}$	1.21	40.47	T

TABLE 1 — *Continued*

ObjID (1)	ra (2)	dec (3)	$z$ (4)	srcid (5)	OAA (6)	counts (7)	Exp. (8)	Targ. (9)	$N_{H}^{Gal}$ (10)	$N_{H}^{Intr.}$ (11)	$\Gamma$ (12)	$f_x$ (13)	$L_X$ (14)	Opt. Class (15)
587731513148571800	32.354515	0.399077	0.061	CXOMP J020925.0+002356	9.9	29.2	2.6	...	2.79	$j0.4$	$1.6^{+0.5}_{-0.5}$	138.82	41.88	T
587731868557377700	168.673538	53.250507	0.106	CXOMP J111441.6+531501	4.8	23.4	16.8	...	0.92	$7.2^{+5.3}_{-2.7}$	$-0.6^{+0.6}_{-0.6}$	43.22	41.96	L
587731873388101721	123.742249	36.890556	0.108	CXOMP J081458.1+365326	8.2	10.6	9.3	...	5.02	$j0.2$	$2.4^{+1.5}_{-1.1}$	10.99	41.09	S
587731886272741666	123.901619	36.765156	0.174	CXOMP J081536.3+364554	6.1	9.3	8.8	...	5.00	$j0.3$	$3.1^{+1.3}_{-1.0}$	10.98	41.30	P
587732050021318723	148.205582	51.884888	0.215	CXOMP J095249.3+515305	1.1	283.2	24.4	I	0.88	$j0.5$	$2.6^{+0.6}_{-0.5}$	59.21	42.60	L
587732135913521261	150.952209	47.631630	0.051	CXOMP J100348.5+473753	0.9	13.5	13.5	...	0.93	$j0.1$	$2.7^{+1.0}_{-0.8}$	4.57	39.90	T
587732469851553889	131.364151	34.419083	0.025	CXOMP J084527.3+342508	4.3	4.6	4.0	...	3.42	$j0.3$	$2.6^{+2.2}_{-1.4}$	7.92	39.56	T
587732482200371401	145.504807	41.440948	0.243	CXOMP J094201.1+412627	6.3	11.4	7.5	...	0.95	$j0.1$	$4.0^{+1.5}_{-1.2}$	6.62	41.01	P
587732484351983843	156.306671	47.115517	0.060	CXOMP J102513.6+470655	10.0	5.8	2.1	...	1.22	$j1.0$	$1.9^{+1.3}_{-1.1}$	31.99	41.16	T
587733397572747445	244.418823	35.004284	0.029	CXOMP J161740.5+350015	0.6	151.7	18.3	I	1.47	$j0.02$	$2.7^{+0.4}_{-0.4}$	35.71	40.29	L
587733603191161025	240.295242	43.194328	0.071	CXOMP J160110.8+431139	7.5	255.5	26.7	...	1.31	$j5.8$	$0.9^{+0.9}_{-0.8}$	294.80	42.47	S
587733604801708195	241.492157	44.05454	0.044	CXOMP J160558.1+440319	3.6	1324.3	4.6	...	1.15	$j0.01$	$1.9^{+0.0}_{-0.0}$	1619.01	42.56	S
587734304342212857	336.311615	-0.364847	0.142	CXOMP J222514.7-002153	7.5	6.2	3.1	...	5.12	$j0.5$	$2.5^{+1.5}_{-1.2}$	29.36	41.76	T
587735348561051857	151.805237	12.787229	0.248	CXOMP J100713.2+124714	4.0	18.0	36.3	...	3.68	$j0.1$	$4.2^{+1.1}_{-1.0}$	2.60	40.55	no-class
587735661546504321	143.357269	34.048050	0.27	CXOMP J093325.7+340252	2.5	33.6	33.6	I	1.47	$j0.03$	$3.6^{+0.6}_{-0.6}$	9.81	39.24	L
587735661546504414	143.272659	34.062729	0.277	CXOMP J093305.4+340345	6.8	23.1	33.6	...	1.47	$j0.4$	$1.5^{+0.6}_{-0.6}$	8.69	42.08	T
587735662089666625	159.883911	39.836349	0.068	CXOMP J103932.1+395010	2.7	10.7	5.0	...	1.43	$j0.9$	$0.8^{+0.7}_{-0.7}$	25.60	41.33	T
587735666377883763	206.114655	56.024902	0.070	CXOMP J134427.5+560129	7.5	45.1	43.5	...	1.09	$0.9^{+0.6}_{-0.4}$	$0.8^{+0.4}_{-0.4}$	16.90	41.19	no-class
587735666377883859	206.093246	55.951073	0.038	CXOMP J134422.3+555703	3.9	7.4	42.7	...	1.09	$j0.2$	$3.2^{+1.3}_{-1.1}$	1.22	38.85	T
587735695377432678	214.062256	53.146236	0.114	CXOMP J141614.9+530846	5.7	8.1	60.5	...	1.27	$j22.5$	$-0.1^{+0.9}_{-1.1}$	3.95	40.99	no-class
587735696440623133	171.764420	56.902294	0.055	CXOMP J112703.4+565408	3.3	7.8	38.3	...	0.92	$j0.5$	$1.5^{+1.3}_{-1.0}$	2.26	40.02	no-class
587735696440623158	171.882370	56.876919	0.005	CXOMP J112731.7+565236	0.8	45.3	39.3	...	0.90	$j0.4$	$0.6^{+0.4}_{-0.4}$	16.00	38.99	H II
587735696440623212	171.780807	56.828369	0.175	CXOMP J112707.3+564942	3.8	12.0	38.3	...	0.91	$j0.1$	$3.8^{+1.6}_{-1.1}$	2.48	40.32	P
587735696448880650	206.089798	55.856201	0.037	CXOMP J134421.5+555122	4.1	9.6	42.7	...	1.08	$j0.2$	$2.2^{+1.2}_{-0.9}$	1.70	39.35	no-class
587735696451371138	215.187088	53.653847	0.117	CXOMP J142044.9+533913	6.4	126.2	4.9	...	1.19	$j0.1$	$1.9^{+0.4}_{-0.3}$	167.86	42.48	S
587735696979656747	180.807953	57.890541	0.034	CXOMP J120313.9+575325	5.9	93.9	57.8	...	1.43	$j0.2$	$1.9^{+0.3}_{-0.2}$	19.12	40.43	H II
587735744228753459	245.066696	29.488642	0.061	CXOMP J162016.0+292919	0.6	10.7	32.2	...	2.74	$j12.6$	$0.1^{+0.7}_{-0.8}$	6.82	40.69	no-class
587736584961196166	205.136429	40.293945	0.171	CXOMP J134032.7+401738	1.2	47.2	43.1	I	0.80	$j0.1$	$2.8^{+0.5}_{-0.4}$	5.02	41.03	P
587736752468394214	241.406998	32.936256	0.053	CXOMP J160537.6+325610	7.7	18.7	19.9	...	2.30	$j0.2$	$1.9^{+0.8}_{-0.7}$	10.33	40.53	T
587736752468394267	241.437714	32.872177	0.115	CXOMP J160545.0+325219	6.0	30.3	20.1	...	2.31	$j0.1$	$2.1^{+0.5}_{-0.5}$	16.30	41.41	no-class
587736781993935128	236.260956	36.156464	0.060	CXOMP J154502.6+360923	3.2	9.8	18.8	...	1.65	$j0.1$	$3.3^{+1.2}_{-1.0}$	2.61	39.55	no-class
587736781993935188	236.282913	36.146473	0.069	CXOMP J154507.8+360847	3.5	12.5	18.8	...	1.65	$j0.1$	$3.6^{+1.3}_{-1.1}$	2.91	39.54	no-class
587736941445447871	216.464218	35.567928	0.186	CXOMP J142551.4+353404	3.2	7.8	50.3	...	1.10	$j0.2$	$3.5^{+1.8}_{-1.6}$	1.20	40.22	S
588007004192637004	243.921677	47.186592	0.198	CXOMP J161541.2+471111	0.5	121.6	3.4	I	1.23	$j0.1$	$1.7^{+0.4}_{-0.3}$	239.03	43.18	T
588007004192637199	243.922241	47.167870	0.197	CXOMP J161541.3+471004	1.4	5.8	3.4	...	1.23	$j0.1$	$3.6^{+3.9}_{-1.6}$	6.97	40.99	P
588007004694839559	119.126747	41.036259	0.072	CXOMP J075630.4+410210	3.3	109.5	6.2	...	4.48	$j0.04$	$2.5^{+0.5}_{-0.4}$	102.97	41.65	L
588007005769957640	120.440094	44.110588	0.131	CXOMP J080145.6+440638	6.6	11.8	9.2	...	4.73	$j0.1$	$3.5^{+1.2}_{-1.0}$	7.35	40.67	P
588010879292932251	173.027710	4.893930	0.150	CXOMP J113206.6+045338	3.4	6.5	6.3	...	3.43	$j0.2$	$3.2^{+2.4}_{-1.4}$	4.43	40.68	no-class
588016891170914329	143.504242	33.990730	0.027	CXOMP J093401.0+335926	5.9	13.6	31.8	...	1.47	$j0.1$	$3.4^{+1.2}_{-1.0}$	4.19	38.94	no-class
588017111297622182	189.892838	47.537556	0.131	CXOMP J123934.2+473215	9.1	82.4	4.5	...	1.13	$2.6^{+0.7}_{-0.6}$	$0.2^{+0.2}_{-0.3}$	434.23	43.15	S
588017111298932927	194.301773	47.330669	0.131	CXOMP J125712.4+471950	2.3	31.3	49.8	...	1.15	$j0.1$	$2.2^{+0.6}_{-0.5}$	3.13	40.78	no-class
588017111833968667	187.945435	47.927235	0.030	CXOMP J123146.9+475538	5.5	9.5	6.5	...	1.17	$j0.7$	$-0.2^{+0.9}_{-1.2}$	34.97	40.81	S
588017567628591240	164.638321	12.720986	0.119	CXOMP J105833.1+124315	6.2	8.8	4.9	...	2.13	$j0.5$	$1.9^{+1.0}_{-0.9}$	29.98	41.76	T

TABLE 1 — *Continued*

ObjID (1)	ra (2)	dec (3)	$z$ (4)	srcid (5)	OAA (6)	counts (7)	Exp. (8)	Targ. (9)	$N_H^{Gal}$ (10)	$N_H^{Intr.}$ (11)	$\Gamma$ (12)	$f_x$ (13)	$L_X$ (14)	Opt. Class (15)
588017569779023967	201.370422	11.335633	0.086	CXOMP J132528.9+112008	5.5	75.7	4.4	...	1.92	j0.2	$1.9^{+0.3}_{-0.3}$	124.39	42.06	S
588017604148133957	186.976318	44.363770	0.276	CXOMP J122754.3+442149	1.7	21.6	4.8	...	1.34	j1.3	$1.4^{+0.5}_{-0.5}$	48.44	42.83	T
588017605772837051	228.612808	36.634247	0.161	CXOMP J151427.0+363803	2.5	21.0	43.5	...	1.35	j0.2	$2.4^{+0.8}_{-0.7}$	2.28	40.80	P
588017625613795424	170.110840	43.255371	0.145	CXOMP J112026.6+431519	7.0	1.8	17.6	...	1.96	j39.4	$-0.7^{+2.1}_{-3.0}$	3.62	41.14	S
588017720102813842	168.741943	40.603119	0.075	CXOMP J111458.0+403611	4.9	22.1	28.3	...	1.94	j0.8	$0.7^{+0.5}_{-0.5}$	10.14	41.03	S
588017722259865662	198.026779	42.690838	0.179	CXOMP J131206.4+424127	3.2	15.4	80.6	...	1.37	j2.2	$-0.3^{+0.7}_{-1.0}$	4.76	41.44	no-class
588017722259865691	198.164169	42.713638	0.111	CXOMP J131239.3+424248	3.0	64.5	90.7	...	1.37	j0.3	$1.6^{+0.3}_{-0.3}$	6.32	41.08	L
588017947748139147	205.227905	40.109875	0.170	CXOMP J134054.6+400635	10.5	917.5	45.1	...	0.79	$0.04^{+0.0}_{-0.0}$	$2.0^{+0.2}_{-0.1}$	154.08	42.80	L
588018089466658843	231.747757	35.976982	0.055	CXOMP J152659.4+355837	0.6	22.4	9.1	I	1.56	j0.1	$2.8^{+0.7}_{-0.6}$	11.71	40.35	T
588295840714129492	185.380676	49.176918	0.184	CXOMP J122131.3+491036	4.4	17.2	72.2	...	1.42	j0.1	$3.1^{+1.0}_{-0.9}$	1.97	40.60	T
588295840714129502	185.415253	49.332184	0.124	CXOMP J122139.6+491955	5.0	15.3	77.0	...	1.44	j3.1	$0.5^{+0.8}_{-0.8}$	4.16	41.09	T
588295842853224515	156.433044	47.326378	0.062	CXOMP J102543.9+471934	5.7	2.9	1.9	...	1.26	j0.3	$3.7^{+2.6}_{-2.0}$	12.03	40.00	P
588297863638089749	126.979630	29.449829	0.029	CXOMP J082755.1+292659	9.8	15.0	14.6	...	3.73	j0.2	$2.3^{+1.3}_{-0.9}$	8.64	39.84	H II
588848898846752926	197.902756	-0.922150	0.083	CXOMP J131136.6-005519	8.6	100.3	20.1	...	1.78	$7.3^{+5.2}_{-3.9}$	$0.2^{+0.7}_{-0.7}$	162.69	42.34	S
588848898846818469	198.065002	-0.930759	0.081	CXOMP J131215.6-005550	4.0	3.6	20.7	...	1.79	j0.2	$4.2^{+2.8}_{-1.8}$	2.26	39.28	P
588848899377529043	183.972015	-0.601967	0.119	CXOMP J121553.2-003607	3.0	8.1	42.0	...	2.08	$0.6^{+1.0}_{-0.6}$	$1.4^{+0.9}_{-0.9}$	2.38	40.75	L
588848899377529068	184.006836	-0.625664	0.121	CXOMP J121601.6-003732	4.9	17.4	41.6	...	2.09	j0.0	$4.9^{+1.1}_{-1.0}$	5.90	39.71	P
588848899387228268	206.030533	-0.475767	0.101	CXOMP J134407.3-002832	0.5	3.6	8.7	...	2.02	j2.5	$1.2^{+1.3}_{-1.2}$	3.75	40.82	T
588848901519179802	170.660416	1.059925	0.075	CXOMP J112238.4+010335	3.4	69.2	18.5	...	4.10	j0.1	$1.8^{+0.3}_{-0.3}$	39.08	41.46	T
588848901519179967	170.649841	1.116308	0.039	CXOMP J112235.9+010658	3.4	6.3	19.9	...	4.11	j0.5	$2.5^{+1.3}_{-1.3}$	3.05	39.58	H II
588848901528289406	191.438202	1.079846	0.106	CXOMP J124545.1+010447	1.1	9.7	6.3	...	1.69	j0.1	$3.5^{+1.3}_{-1.1}$	6.31	40.35	T
588848901531107518	197.878723	1.184934	0.070	CXOMP J131130.8+011105	8.5	24.7	4.5	...	1.97	$15.1^{+8.5}_{-5.8}$	$-1.5^{+0.7}_{-0.8}$	270.20	42.40	S

NOTE. — (1) SDSS Object ID. (2) and (3) J2000 epoch. (4) spectroscopic redshift. (5) ChaMP X-ray source ID, expressed as CXOMP Jhhmmss.s+/-ddmmss, using the truncated X-ray source position. (6) *Chandra* off-axis angle in arcmin; (7) net 0.5 – 8 keV source counts. (8) Vignetting-corrected exposure time in ksec. (9) I = intended *Chandra* PI target. (10) Galactic column in units of  $10^{20}$   $\text{cm}^{-2}$ . (11) Best-fit YAXX intrinsic column density in  $10^{22}$   $\text{cm}^{-2}$ ; upper limits are at 90% confidence level and errors represent  $1-\sigma$  uncertainties. (12) Best-fit YAXX power-law index  $\Gamma$ ; errors represent  $1-\sigma$  uncertainties. (13) X-ray flux (0.5 – 8 keV) in units of  $10^{-15}$   $\text{erg s}^{-1} \text{cm}^{-2}$ . (14) log X-ray luminosity (0.5 – 8 keV) in  $\text{erg s}^{-1}$ . (15) Optical spectral classification, S = Seyfert, L = LINER, T = Transition Object, P = Passive galaxy; see text for details. Note that only for objects with  $\geq 200$  counts,  $N_H^{Intr.}$  and  $\Gamma$  values are the result of fitting simultaneously a power-law and absorption.



TABLE 2  
OBJECT SAMPLE STATISTICS.

Sample	$N_{\text{opt}}$ (fraction <sup>a</sup> ,%)	$N_{\text{X-ray det.}}$ (fraction <sup>b</sup> ,%)	$N_{\text{X-ray det.}}/N_{\text{opt}}$ (%)
H II	498 (27.6)	7 (6.5)	$1.4 \pm 4.5$
Seyfert	28 ( <b>1.5</b> )	18 ( <b>16.8</b> )	<b><math>64.3 \pm 18.9</math></b>
Transition	194 (10.7)	32 (29.9)	$16.5 \pm 7.2$
LINER	70 (3.9)	13 (12.1)	$18.6 \pm 11.9$
some emission–no class	558 (31.1)	19 (17.8)	$3.4 \pm 4.2$
Passive	459 (25.4)	18 (16.8)	$3.9 \pm 4.6$

NOTE. — The quoted errors represent standard deviations assuming Poisson statistics.

<sup>a</sup> Fraction by type of all 1807 SDSS galaxies on ACIS chips, which excludes those falling on  $ccd = 8$ , and with  $\theta > 0.2$  deg.

<sup>b</sup> Fraction of all 107 X-ray detected SDSS galaxies.

TABLE 3  
 $\Gamma - L/L_{\text{edd}}$  - CORRELATION COEFFICIENTS AND SIGNIFICANCE

Sample	$r_s$	Prob.	N
for $L_X = L_X(0.5 - 8)$ keV .....			
all	<b>-0.52</b>	$< 1.0 \times 10^{-3}$	107
Seyfert	-0.18	0.43	18
Transition	-0.29	0.11	31
LINER	-0.39	0.18	13
for $L_X = L_X(2 - 10)$ keV .....			
all	<b>-0.75</b>	$< 1.0 \times 10^{-3}$	107
Seyfert	-0.36	0.12	18
Transition	<b>-0.52</b>	$2.3 \times 10^{-3}$	31
LINER	<b>-0.56</b>	$4.4 \times 10^{-2}$	13

NOTE. — The Spearman-rank test correlation coefficient, chance probability, and number of sources for each correlation/sample respectively. The most significant probabilities for anticorrelations (chance probability less than 5%) are shown in boldface.

TABLE 4  
 $\Gamma - L/L_{\text{edd}}$  - LINEAR REGRESSION COEFFICIENTS

Sample	Slope	Intercept	$\chi^2/\text{dof}$
for $L_X = L_X(0.5 - 8)$ keV .....			
all	$-0.16 \pm 0.04$	$1.36 \pm 0.13$	309/105
all, no passive, no HII	$-0.07 \pm 0.05$	$1.51 \pm 0.15$	235/81
all with $L_X \gtrsim 10^{42}$ erg s <sup>-1</sup>	$0.12 \pm 0.12$	$2.09 \pm 0.29$	83/17
Seyfert	$0.94 \pm 0.15$	$3.59 \pm 0.35$	89/16
Transition	$-0.001 \pm 0.11$	$1.88 \pm 0.37$	21/29
LINER	$-0.20 \pm 0.09$	$1.42 \pm 0.34$	29/11
for $L_X = L_X(2 - 10)$ keV .....			
all	$-0.27 \pm 0.04$	$0.98 \pm 0.13$	274/105
all, no passive, no HII	$-0.21 \pm 0.05$	$1.11 \pm 0.15$	219/81
all with $L_X \gtrsim 10^{42}$ erg s <sup>-1</sup>	$-0.19 \pm 0.14$	$1.28 \pm 0.36$	95/16
Seyfert	$0.42 \pm 0.18$	$2.49 \pm 0.43$	119/16
Transition	$-0.09 \pm 0.10$	$1.57 \pm 0.38$	21/29
LINER	$-0.25 \pm 0.09$	$1.18 \pm 0.34$	26/11

NOTE. — The slope, intercept,  $\chi^2$ , and degrees of freedom (dof) for the best error-weighted linear fits for the whole sample of X-ray detected galaxies, and per spectral type. Errors are at 1- $\sigma$  confidence levels.

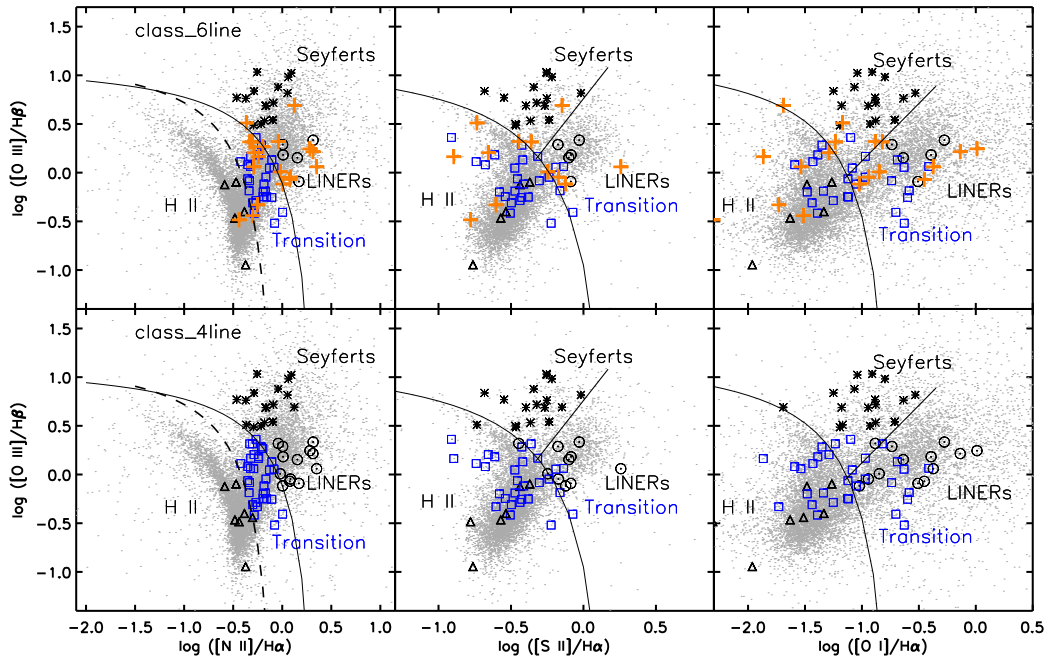


FIG. 1.— Diagnostic diagrams for all ChaMP galaxies that exhibit emission-line activity, with relatively high ( $> 2$ ) signal-to-noise line flux measurements in all 6 lines (*top*), and in only [N II], [O III],  $H\beta$ , and  $H\alpha$  (*bottom*). The solid and dashed black curves illustrate the Kewley et al. (2001) and Kauffmann et al. (2003b) separation lines while the diagonal lines illustrate the separation between Seyferts and LINERs by Kewley et al. (2006). The grey points correspond to galaxies in ChaMP fields that fall on or near the ChaMP ACIS chips, but are not necessarily X-ray detected. Seyferts, Liners, Transition Objects, and H II galaxies are shown as asterisks, open circles, blue squares, and triangles, respectively. The orange crosses are 6-line non-classified objects with a 4-line class. It is quite apparent that the combination of the 4-line classification and X-ray detection is very efficient in distinguishing between different types of emission among LLAGN, quantitatively identical to the 6-line method.

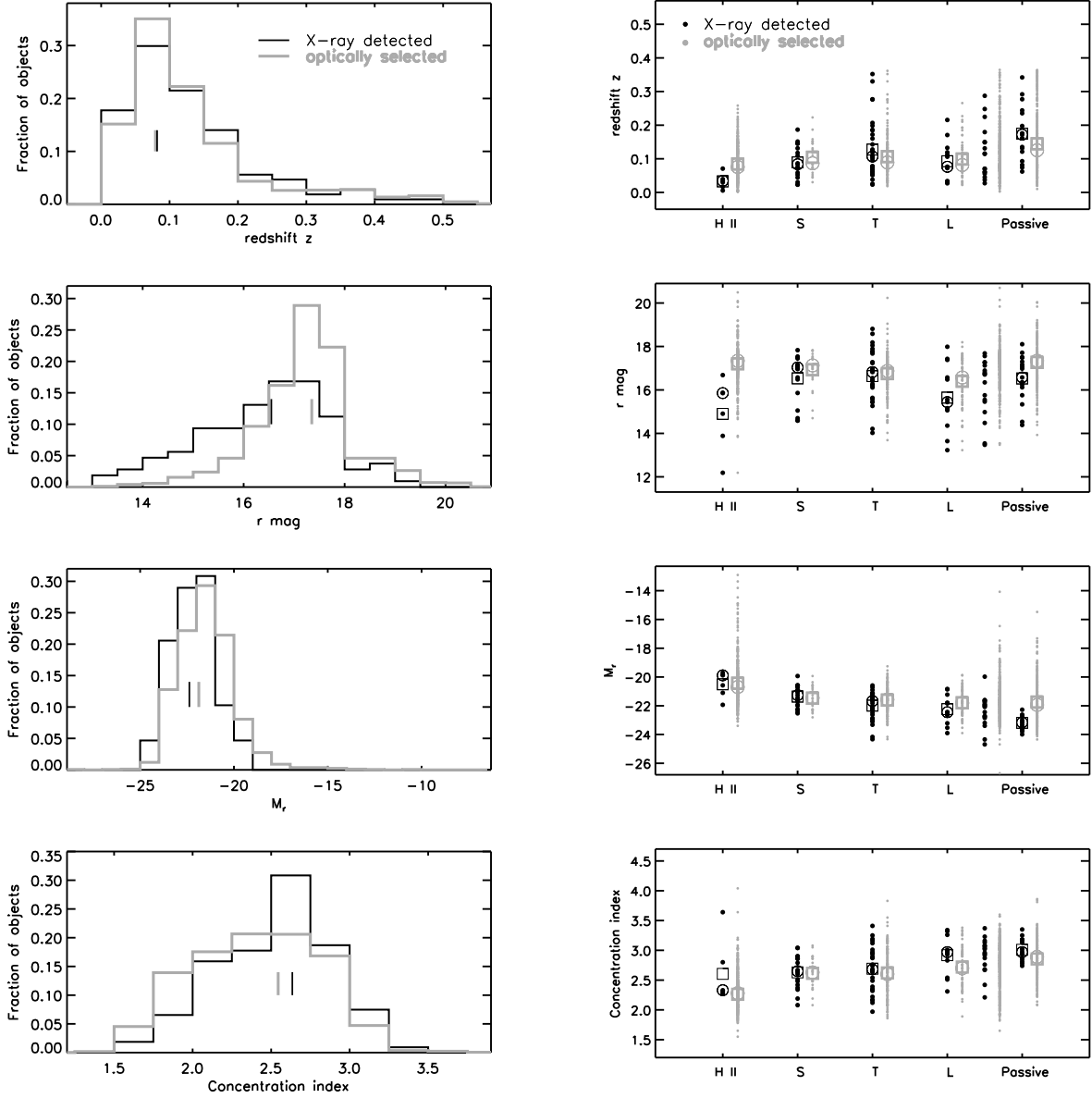


FIG. 2.— Comparison of the optical properties of X-ray detected galaxies and all optically selected (SDSS) galaxies on or near ChaMP fields/chips. *Left*: Histograms of redshift ( $z$ ), apparent  $r$ -band magnitude ( $m_r$ ), absolute  $r$ -band magnitude ( $M_r$ ), and the concentration index ( $C$ ) for the full samples of SDSS galaxies on/near ChaMP fields and the ChaMP detections; median values are indicated by the vertical bars. *Right*: Individual measurements of  $z$ ,  $m_r$ ,  $M_r$  and  $C$  are shown separately per galaxy spectral type; both average (squares) and median (circles) values are indicated here, for all types of objects. The bias caused by the X-ray detection criterion is clearly weak; the few X-ray detected HII's dominate the observed difference in  $r$  and  $M_r$  distributions.

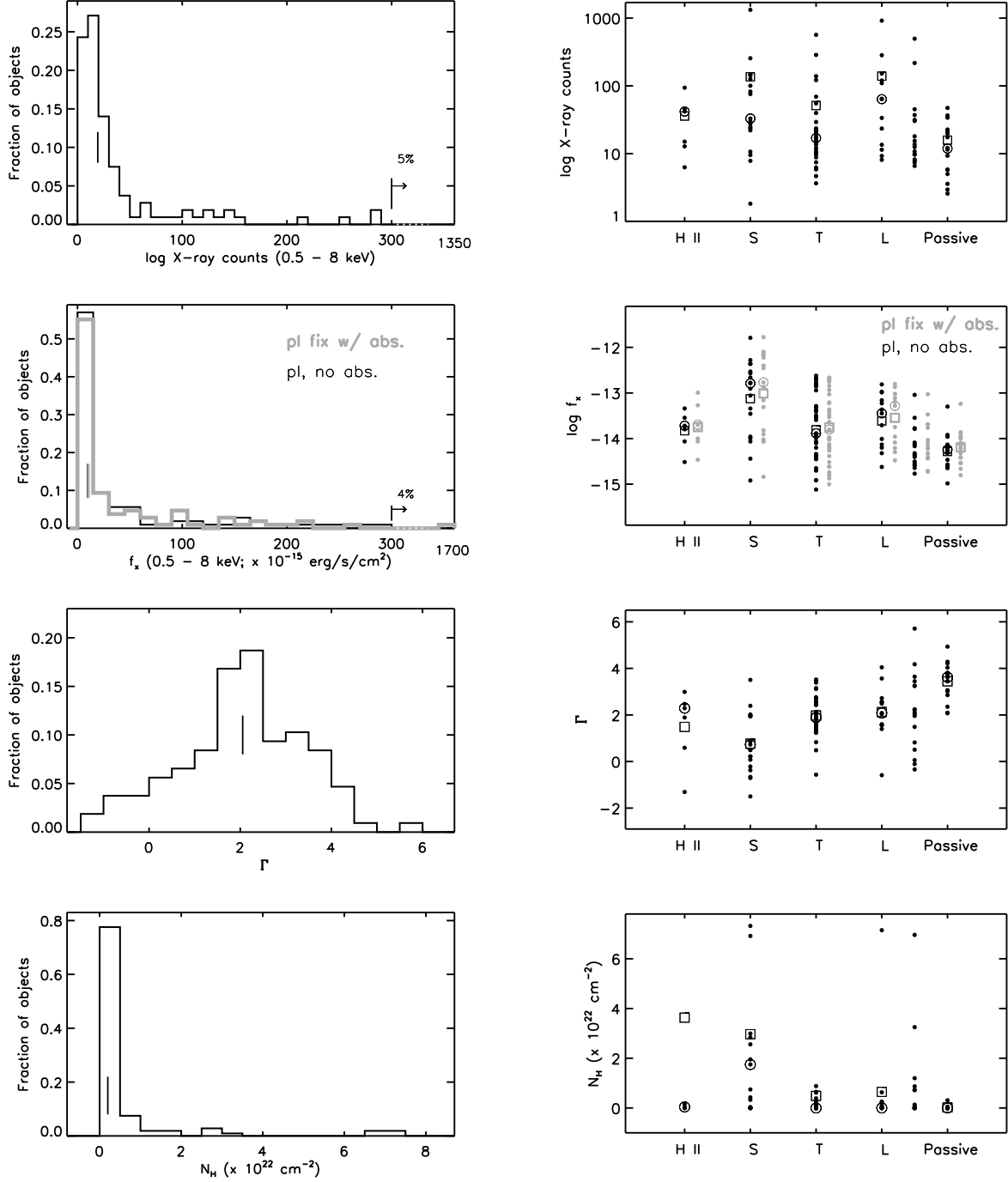


FIG. 3.— Distribution of X-ray properties of the ChaMP galaxies. *Left:* Histograms of X-ray counts in the 0.5 – 8 keV regime, the X-ray flux  $f_x$  (calculated via two fitting models, a power-law with no intrinsic absorption and a fixed power-law with variable absorption), the (best) X-ray photon index  $\Gamma$ , and the (best)  $N_H$  (see text); median values are indicated by the vertical bars. *Right:* Individual measurements of X-ray counts,  $f_x$ ,  $\Gamma$ , and  $N_H$  shown separately per galaxy spectral type; average and median values are indicated for all types of objects by squares and circles respectively.

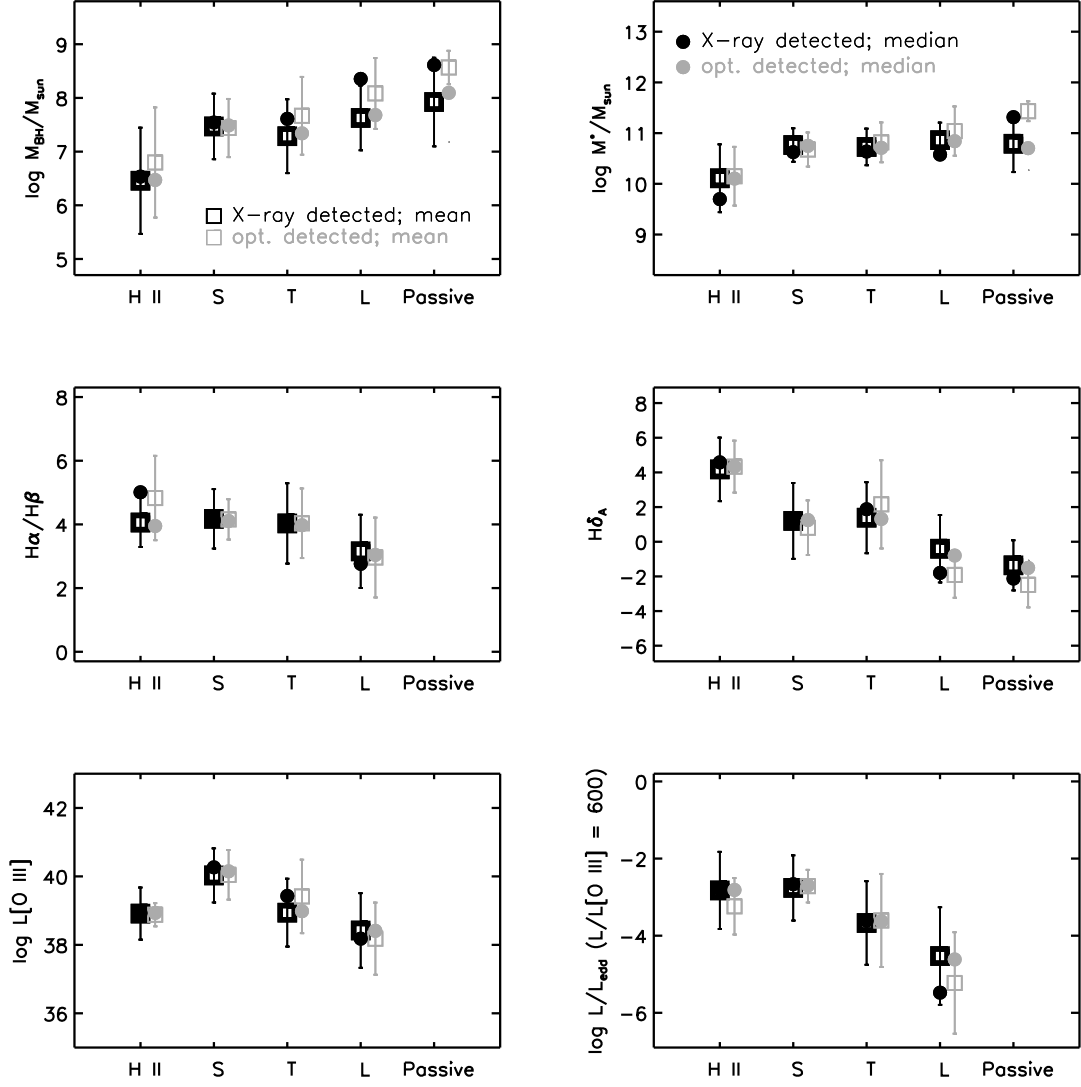


FIG. 4.— Comparison of median and average optical properties of X-ray detected galaxies and all optically selected galaxies on or near ChaMP fields/chips, along the  $H\text{ II} \rightarrow S \rightarrow T \rightarrow L \rightarrow \text{passive galaxies}$  sequence. The plots show: the BH mass (based on  $M_{\text{BH}} - \sigma_*$  relation of Tremaine et al. 2002), the (dust corrected) stellar mass ( $\log M_*/M_{\odot}$ ), the Balmer decrement, the  $H\delta_A$  Balmer absorption-line index,  $L[\text{O III}]$ , and the accretion rate expressed by  $L_{\text{bol}}/L_{\text{Edd}}$ , where  $L_{\text{bol}}/L[\text{O III}] = 600$ ; average and median values are indicated by squares and circles respectively.

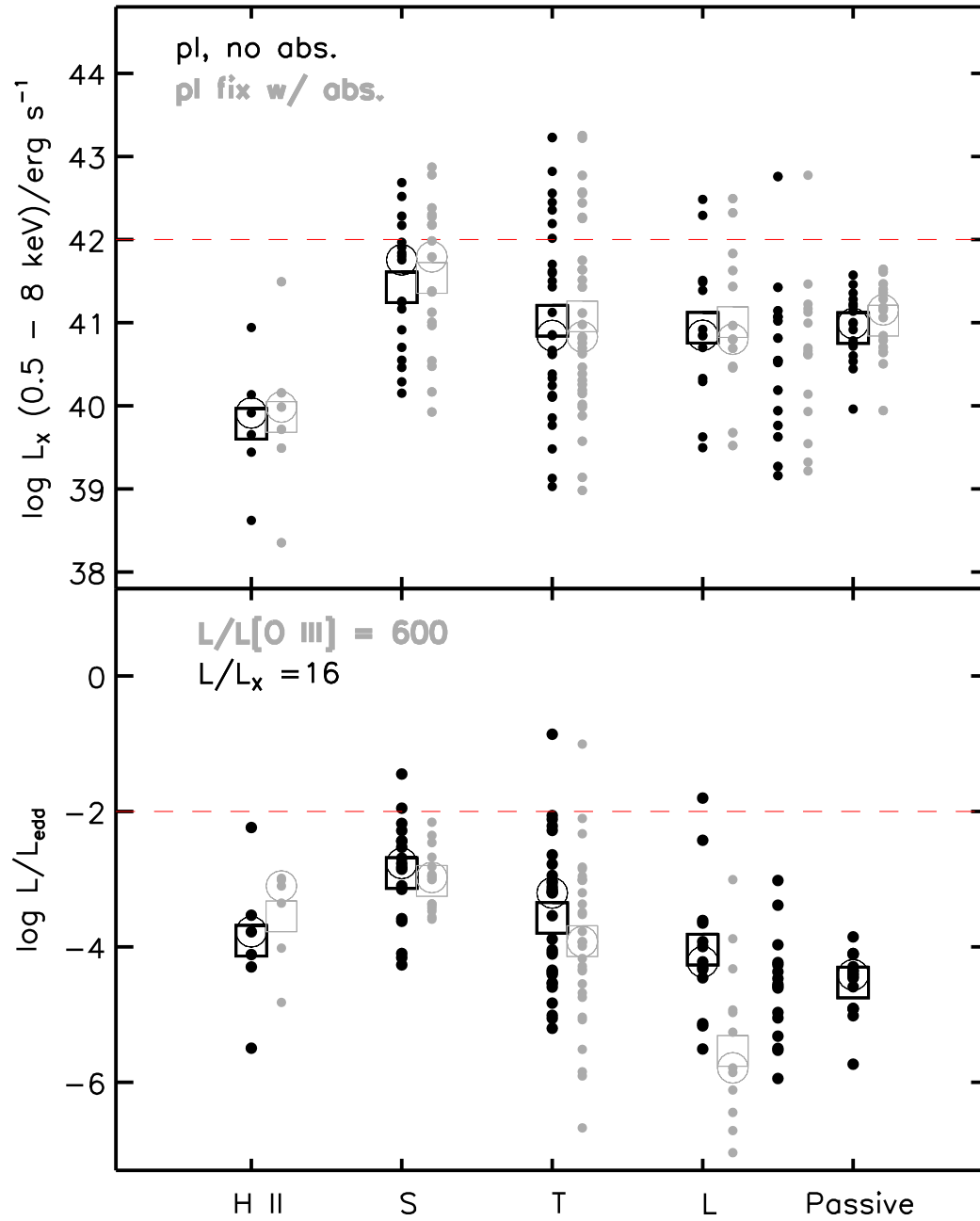


FIG. 5.— The  $H \text{ II} \rightarrow S \rightarrow T \rightarrow L \rightarrow \text{passive galaxies}$  sequence in X-ray: the X-ray luminosities obtained via *yaxx* for two fitting models (1. a power-law with no intrinsic absorption and 2. a fixed power-law with  $\Gamma = 1.9$  with intrinsic absorption); the accretion rate values, expressed by  $L/L_{\text{Edd}}$ , calculated using both  $L_{\text{bol}}/L_X = 16$  and  $L_{\text{bol}}/L[\text{OIII}] = 600$  are compared; average and median values are indicated by squares and circles respectively.

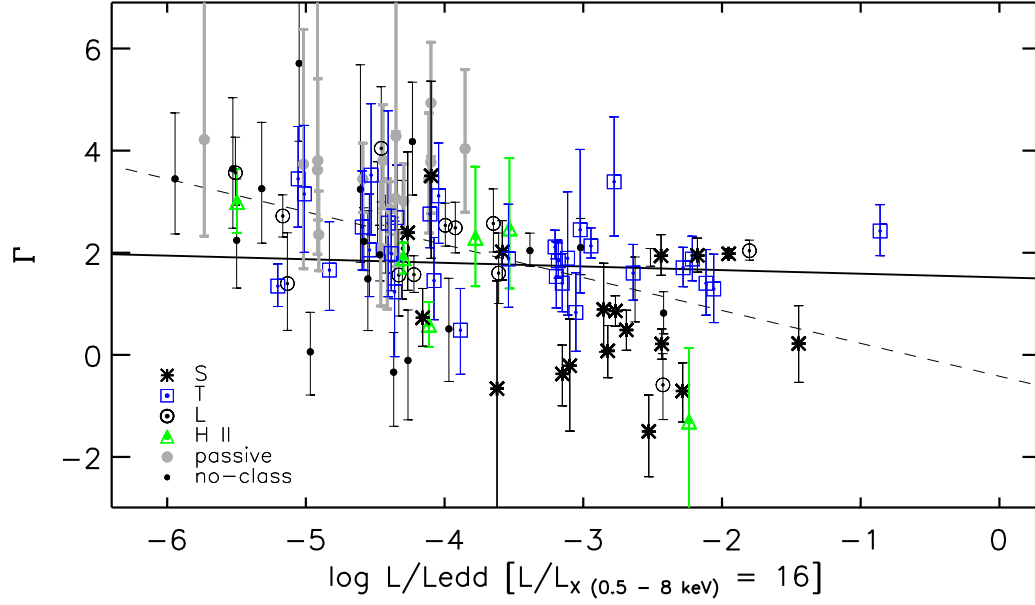


FIG. 6.— Distribution of the X-ray photon index as a function of  $L/L_{\text{edd}}$  where  $L = L_{\text{bol}}$  is estimated using  $L_{\text{bol}}/L_X = 16$ . There is clearly apparent an anti-correlation between these two measures; the symbols reflect the different spectral optical classification. The solid and dotted lines reflect the best fit linear relations with the errors weighted and not weighted, respectively.

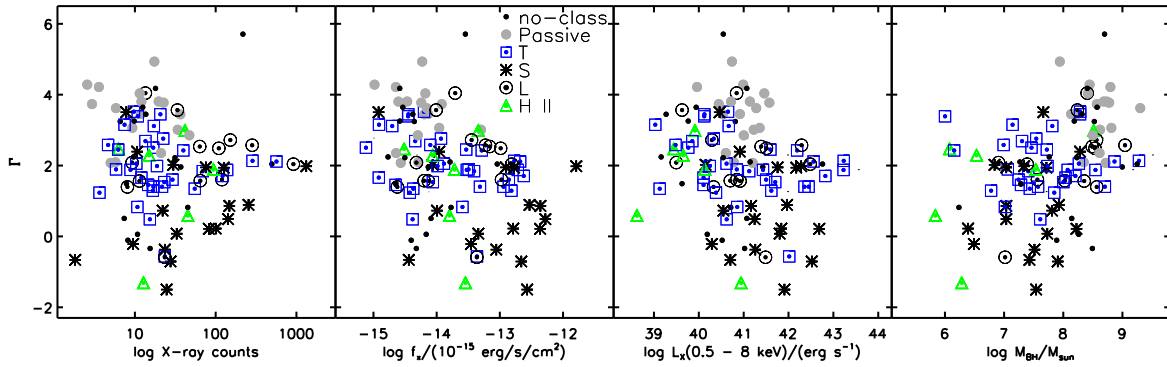


FIG. 7.— The relation between the 0.5 – 8 keV X-ray photon index and the total number of counts, the 0.5 – 8 keV flux  $f_x$ , the 0.5 – 8 keV luminosity  $L_X$ , and the BH mass. No relation appears to exist between  $\Gamma$  and X-ray counts, while there are rather weak apparent negative correlations with  $f_x$  and  $L_X$ ;  $M_{\text{BH}}$  does not appear to correlate with  $\Gamma$ .

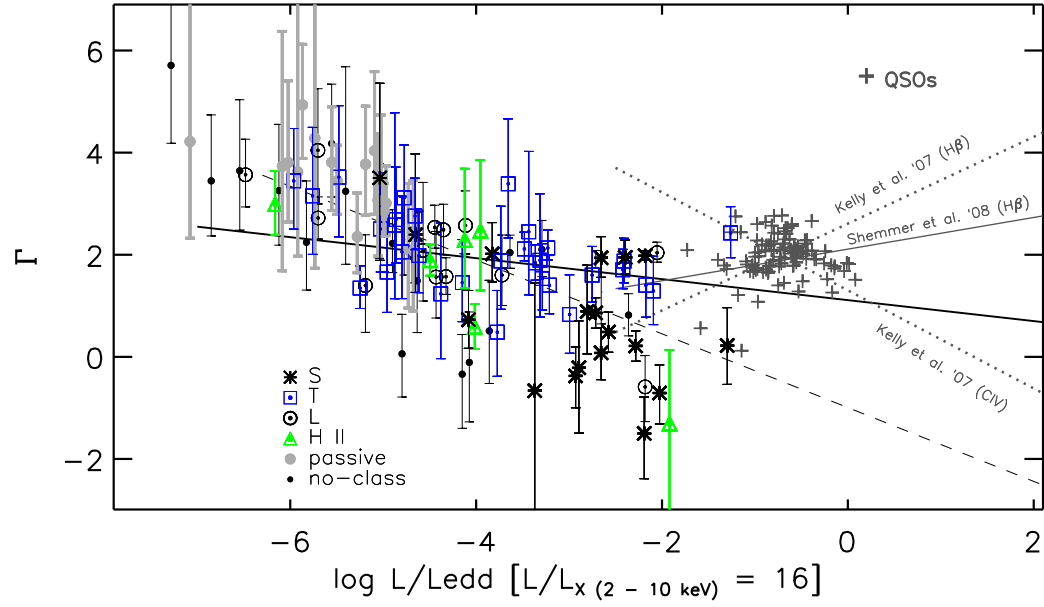


FIG. 8.— Distribution of the X-ray photon index  $\Gamma$  as a function of  $L/L_{\text{edd}}$  where  $L = L_{\text{bol}}$  is estimated using  $L_{\text{bol}}/L_X = 16$ , with  $L_X = L_X(2 - 10\text{keV})$  calculated from  $L_X(0.5 - 8\text{keV})$  using  $\Gamma$ . We show for comparison the measurements of  $\Gamma$  and  $L/L_{\text{edd}}$  for the ChaMP (high  $z$ ) SDSS QSOs with spectra (Green et al. 2009), where both  $\Gamma$  and  $L/L_{\text{edd}}$  are calculated in the same way as for the ChaMP galaxies/LLAGN, with the difference that the bolometric correction for quasars is considered to be  $L_{\text{bol}}/L_X = 83$ , independent of their luminosity.